Since January 2020 Elsevier has created a COVID-19 resource centre with free information in English and Mandarin on the novel coronavirus COVID-19. The COVID-19 resource centre is hosted on Elsevier Connect, the company's public news and information website.

Virology 577 (2022) 1–15

Contents lists available at ScienceDirect

Virology

journal homepage: www.elsevier.com/locate/virology

Multi-target direct-acting SARS-CoV-2 antivirals against the nucleotide-binding pockets of virus-specific proteins

Ruchi Rani [a], Siwen Long [b], Akshay Pareek [a], Preeti Dhaka [a], Ankur Singh [a], Pravindra Kumar [a], Gerald McInerney [b], Shailly Tomar [a,*]

[a] Department of Biosciences and Bioengineering, Indian Institute of Technology Roorkee, Roorkee, Uttarakhand, India
[b] Department of Microbiology, Tumor and Cell Biology, Karolinska Institutet, SE-17177 Stockholm, Sweden

ARTICLE INFO

Keywords:
SARS-CoV-2
Nucleotide-binding pocket
In silico
Drug repurposing
Antivirals

ABSTRACT

The nucleotide-binding pockets (NBPs) in virus-specific proteins have proven to be the most successful antiviral targets for several viral diseases. Functionally important NBPs are found in various structural and non-structural proteins of SARS-CoV-2. In this study, the first successful multi-targeting attempt to identify effective antivirals has been made against NBPs in nsp12, nsp13, nsp14, nsp15, nsp16, and nucleocapsid (N) proteins of SARS-CoV-2. A structure-based drug repurposing *in silico* screening approach with ADME analysis identified small molecules targeting NBPs in SARS-CoV-2 proteins. Further, isothermal titration calorimetry (ITC) experiments validated the binding of top hit molecules to the purified N-protein. Importantly, cell-based antiviral assays revealed antiviral potency for INCB28060, darglitazone, and columbianadin with EC_{50} values 15.71 μM, 5.36 μM, and 22.52 μM, respectively. These effective antivirals targeting multiple proteins are envisioned to direct the development of antiviral therapy against SARS-CoV-2 and its emerging variants.

1. Introduction

The emergence of SARS-like respiratory illness in the Wuhan province of China in December 2019, resulted in the identification of a novel strain of coronavirus (CoV) named as SARS-CoV-2. The World Health Organization (WHO) declared coronavirus disease 2019 (COVID-19) pandemic on March 11, 2020, because of its high transmission dynamics and high infection rate. Despite of its rapid global spread, the assessed fatality rate of SARS-CoV-2 is 6.6% that is lower than SARS-CoV (9.6%) and Middle East Respiratory Syndrome Coronavirus (MERS-CoV) 34.3% (Wang et al., 2020).

Coronaviruses belong to the family *Coronaviridae* in the order *Nidovirales* infecting humans, birds, and livestock (Drexler et al., 2014). They are further classified into four subgroups namely alpha (α), beta (β), gamma (γ), and delta (δ) CoVs. Human CoV (hCoV-HKU1 and hCoV-OC43), Middle East Respiratory Syndrome (MERS) (de Groot et al., 2013; Zaki et al., 2012) SARS (Ksiazek et al., 2003; Kuiken et al., 2003) and, SARS-CoV-2 belong to β-CoV while the other hCoV strains 229E and NL63 belong to α-CoV (Hui et al., 2020; Ju et al., 2020a). α-CoV and β-CoV infect mammalian species, while γ-CoV and δ-CoV infect avian species. Among these strains, SARS-CoV, MERS-CoV, and SARS-CoV-2 are associated with acute human respiratory disease, while the other strains (229E, OC43, NL63, and HKU1) exhibit moderate clinical signs such as nasal discharge, fever, sore throat, and cough (Zhou et al., 2020).

SARS-CoV-2 is a non-segmented, enveloped, positive-sense single-stranded RNA (+ ss RNA) virus that has a large genome of ~30 kb containing 14 open reading frames (ORFs) (Gordon et al., 2020; Wu et al., 2020). The 5′ end of the genome has two ORFs 1a and 1b that covers two-third of genome and encodes two polyproteins; pp1a and pp1ab. These polyproteins are auto-proteolytically processed into nsp1-nsp16 and form different virus replicase complexes (Chan et al., 2020). The remaining 3′ one-third genome encodes four structural proteins: spike (S), membrane (M), envelope (E), and nucleocapsid (N) (Wu et al., 2020). SARS-CoV-2 has evolved over time with more than 40,000 genomic variants and 353,341 mutation events compared to the Wuhan reference genome since its emergence in 2019 (Mercatelli and Giorgi, 2020). Most of the mutations are neutral, meaning that they do not affect the properties of virus while some have raised concerns because they allow the virus to bypass host immune responses (Sette and Crotty, 2021). Whereas, some of these mutations in the spike protein have strengthened the affinity between the S-protein and its receptor,

* Corresponding author.
E-mail address: shailly.tomar@bt.iitr.ac.in (S. Tomar).

https://doi.org/10.1016/j.virol.2022.08.008
Received 24 June 2022; Received in revised form 20 August 2022; Accepted 20 August 2022
Available online 7 October 2022

the human angiotensin-converting enzyme 2 (ACE2) (Ali et al., 2021), some have enhanced viral pathogenesis and increased the transmission rate of SARS-CoV-2 (Huang et al., 2020; Singhal, 2020; Zhang et al., 2020). Although the virus transmission has been confined due to continued monitoring, awareness, preparedness and vaccination, SARS-CoV-2 antiviral medications are required to combat recurrence and emergence of new variants of concern.

Over the past two decades of pharmaceutical research and development, atomic structures of proteins and structure-assisted drug discovery have directly contributed to the identification and optimization of lead drug molecules. In response to the pandemic, structural biologists around the world in a short time period have determined 3D structures of almost all the SARS-CoV-2 proteins, and those structures are being exploited for structure-based drug discovery. The Protein Data Bank (PDB) identification numbers of SARS-CoV-2 structural and non-structural proteins, along with their roles in virus life cycle are listed in Supplementary Table 1.

Generally, the nucleotide binding pockets (NBPs) in viral proteins form essential molecular interactions with nucleotide triphosphates (NTPs) during viral replication. These NBPs are conserved within a viral family, and are thus attractive targets for identification, design and development of antivirals (Ju et al., 2020b). Atomic structures of virus proteins in complex with nucleotides as well as nucleotide analog drugs are available for different viruses such as dengue virus (PDB ID: 4HDG), enterovirus (PDB ID: 3N6M), Bombyx mori cypovirus 1 (PDB ID: 3JB6) and others. In these structures mostly the NBPs of essential viral proteins such as RNA-dependent RNA polymerase (RdRp), helicase, methyltransferase (MTase) or nucleocapsid (N) have been targeted. The US Food and Drug Administration (FDA) has authorized antiviral drug molecules against different viruses, such as azidothymidine (AZT), the first anti-HIV/AIDS drug against HIV's reverse transcriptase (RT) (Árquez et al., 2020; Parker and Masters, 1990). Tenofovir has replaced AZT for HIV/AIDS and hepatitis B virus (HBV) (Masho et al., 2007). Sofosbuvir (anti-hepatitis C directed against hepatitis C virus (HCV) RdRp) (Temesgen et al., 2014), acyclovir (anti-herpes simplex viruses (HSV) family against viral DNA polymerase) (Kimberlin and Whitley, 2007), entecavir (anti-HBV viral polymerase) (Dimou et al., 2007), lamivudine (anti-HBV and anti-HIV by targeting RT enzyme) (Anderson and Rower, 2010) and various other antiviral drugs. These medications are nucleotide derivatives that compete with the physiological nucleotides for binding to the NBPs of the viral proteins.

For multi-targeticity and rapid identification of efficacious antivirals against SARS-CoV-2, we envisioned a strategy to repurpose pharmacologically active compounds that bind to the NBPs of several SARS-CoV-2 proteins. NBPs of six different SARS-CoV-2 proteins-nsp12 (Gao et al., 2020), nsp13 (Mirza and Froeyen, 2020), nsp14 C-terminal domain (CTD) and N-terminal domain (NTD) (Ma et al., 2015), nsp15 (Kim et al., 2020), nsp16 (Rosas-Lemus et al., 2020), and N protein (Chang et al., 2014) were targeted.

NBPs in these viral proteins have been identified and characterized by determining the atomic structures, which are available in the PDB database. A structure-assisted *in silico* virtual screening of three different libraries: Selleckchem FDA approved drug library, Selleckchem natural product library (NPL) and Library of Pharmacologically Active Compound - Sigma (LOPAC) was performed for identification of potential small molecules with multi-target characteristics. Computer-aided screening of compound libraries using single molecule multi-target (SMMT) approach identified number of promising hits. Furthermore, the identified molecules were analysed using isothermal titration calorimetry (ITC) to measure binding parameters such as affinity and kinetics of the antiviral compounds. Finally, cell-based SARS-CoV-2 assays confirmed antiviral activity of a subset of these compounds. This report is the first study of effective and promising repurposed drug molecules with multi-targeticity against SARS-CoV-2.

2. Materials and methods

2.1. Computer-aided structure-based virtual screening

All structure related information for SARS-CoV-2 proteins were obtained from the Research Collaboratory for Structural Bioinformatics (RCSB) PDB data base (Berman et al., 2000). SwissADME online tool was used for *in silico* drug-likeness analysis (Daina et al., 2017). A BOILED-Egg to predict gastrointestinal absorption and brain penetration of small molecules (Daina and Zoete, 2016).

The coordinates of the three-dimensional structure of six proteins of SARS-CoV-2 (nsp12, nsp13, nsp14, ns15, nsp16, and N) were downloaded in.pdb format from RCSB PDB. The downloaded files with.pdb format were converted to.pdbqt format by removing water molecules, adding hydrogen and gasteiger charges using AutoDock MGL tools 1.5.6 (Morris et al., 2009). To identify potential antiviral compounds, three drug libraries i.e. FDA-approved drug library and NPL from Selleckchem (2747 and 2370 compounds respectively) and LOPAC^{1280} from Sigma (1280 compounds) were retrieved in.sdf format and converted to AutoDock ligand (.pdbqt) format after energy minimization using open Babel in PyRx 0.8 algorithm (Dallakyan and Olson, 2015; O'Boyle et al., 2011). The virtual screening was performed using PyRx 0.8 algorithm in the macOS Mojave workstation. The NBP residues of different proteins with grid box parameters for screening are mentioned in Table 1.

2.2. Molecular docking of compounds

Molecular docking was performed for the nucleotide monophosphate (NMPs) (AMP, CMP, GMP, and UMP), NTPs (ATP, CTP, GTP, and UTP), and remdesivir. Remdesivir, a nucleotide prodrug of an adenosine analog along with NMPs and NTPs were used as positive controls. The binding energies (BE) of virtually screened ligand molecules were compared with the positive controls and molecules with BE $\geq$ 6 kcal/mol were selected. Further, the selected ligand molecules were subjected to molecular docking using the AutoDock Vina algorithm (Trott and Olson, 2010) for detail analysis. The grid box parameters for molecular docking are given in Table 1.

2.3. In silico analysis for drug-likeness

Molecule toxicity range and pharmacokinetic properties are two important criteria required for the acceptance of any molecule as a drug candidate. Using SwissADME online tool (Daina et al., 2017), these properties were characterized for the selected molecules. The canonical simplified molecular input line entry system (SMILES) string of selected ligands was retrieved from PubChem and submitted into the SwissADME online server tool. The output result was depicted as bioavailability radar, which follows the selection of the desirable compounds in the early phases of the drug discovery. The different physicochemical properties SIZE (in kDa), POLAR {polarity as topological polar surface area (TPSA)}, FLEX (flexibility by the number of rotatable bonds), INSAT (saturation), and LIPO (lipophilicity) have been studied. Along with the six sets of parameters, it includes other parameters like Lipinski's rule of five for the betterment of the drug-likeness studies (Lipinski et al., 1997). Similarly, the prediction of compounds for the gastrointestinal (GI) absorption or blood-brain barrier (BBB) permeation, as well as P-glycoprotein (Pgp) substrate/non-substrate analysis, was done using the BOILED-Egg (Brain Or IntestinaL EstimateD permeation) model (Daina and Zoete, 2016).

2.4. Ligand-target interaction analysis and visualization

The molecular interaction of ligands with the SARS-CoV-2 target proteins was visualized and analysed using PyMOL 2.3.4 and LIGPLOT^{+} for two-dimensional graphical representation of protein-ligand interactions (Wallace et al., 1995). A comparative study of the molecular

Table 1
Nucleotide-binding site residues of SARS-CoV-2 protein and grid box parameters for virtual screening and molecular docking.

Proteins (PDB ID)	Residues	Center (Å) (X, Y, Z)	Dimensions for screening (Å) (X, Y, Z)	Dimensions for Vina (Å) (X, Y, Z)
nsp12 (6M71)	Asp760, Asp761, Asn691, Ser682, Thr680, Asp623, Asp618, Val557, Arg555	116.7604 116.5054 128.0258	19.6447, 23.5576, 27.8883	64, 70, 74
nsp13 (6ZSL)	Lys288, Ser289, Asp374, Glu375, Gln404, Arg567	−14.6949 14.1970 −75.2021	13.4579, 17.5720, 18.5686	40, 47, 52
nsp14 (5C8S) **NTD**	Asp27, Asp90, Glu92, Glu191, His268,	1.0235, −1.0583, 28.0886	21.2173, 13.6721, 12.9231	62, 35, 36
CTD	Trp292, Asn306, Arg310, Asp331, Gly333, Pro335, Lys336, Asp352, Trp385, Asn386, Val389, Phe401, Tyr420, Asn422, Phe426, Thr428, Phe506	6.0228, −28.8145, 6.9992	20.8847, 26.5642, 24.5406	60, 69, 66
nsp15 (6VWW)	His235, His250, Lys290, Thr341, Tyr343, Ser294	−92.0340, 20.9831, −30.7497	13.7609, 17.4511, 19.5213	34, 48, 46
nsp16 (6W4H)	Lys6844, Asp6928, Lys6968, Glu7001, Asn6841, Tyr6845, Gly6869, Ala6870, Ser6872, Gly6879, Asp6897, Asn6899, Leu6898, Asp6912, Met6929	83.3018, 17.3976, 26.0466	17.3564, 25.2003, 17.6516	50, 72, 50
N (6VYO)	Ser51, Phe53, Ala55, Ala90, Arg107, Tyr109, Tyr111, Arg149	−12.1982, 11.5831, 19.5713	16.3450, 21.5780, 19.1638	40, 48, 48

interaction pattern of hydrogen bond acceptor (HBA) and hydrogen bond donor (HBD) moieties of positive control (i.e., GMP) with ligands were done.

2.5. Isothermal titration calorimetry (ITC)

Expression and purification for SARS-CoV-2 N-protein (residues 1-174, the N-terminal domain/NTD) was done using the protocol reported by (Dhaka et al., 2022). In brief, the N-protein was cloned in pET28c vector and was over-expressed using *E. coli* expression system, and purified by Ni-NTA affinity chromatography. Purified proteins were concentrated to ~3.6 mg/mL and used in the ITC experiments. The thermodynamic binding titration experiments were carried out to evaluate binding of selected molecules to purified N-protein of SARS-CoV-2 using MicroCal ITC200 micro calorimeter (Malvern, Northampton, MA). The titrations of ligands and protein were performed at 25 °C using buffer containing 20 mM Tris (pH 8.0) and 20 mM NaCl. All ligand molecules used in this study were purchased from Cayman (Olaparib (10621); VX-809 (22196); INCB28060 (20056); Paliperidone (15556); Flibanserin (19203); SN 38 (15632); Bicuculline (11727); Columbianadin (27661)) except for darglitazone sodium, which was procured from Sigma (Catalogue no. SML0977). Table 2 lists the various set parameters and all selected ligands and protein concentrations used in the ITC experiment by keeping all other parameters equal. The data of binding isotherms (ΔH, ΔS, and K_D values) were fitted by single-site binding model and processed using MicroCal Analysis Software, Malvern in association with commercially available Origin 7.0 program.

2.6. Cell lines and virus

Vero-E6 cells (ATCC-CRL-1586) were maintained in Dulbecco's Modified Eagle Medium (DMEM) (Sigma) supplemented with 10% fetal bovine serum (Sigma), 1% penicillin–streptomycin (Sigma) and 1% L-glutamine (Gibco). Cells were cultured at 37 °C in a humidified incubator with 5% CO_2. SARS-CoV-2, isolated from the first Swedish patient, was received from the Public Health Agency of Sweden. All work with infectious virus was performed in the Biomedicum Biosafety Level 3 core facility, Karolinska Institutet.

Table 2
Different parameters and concentrations of protein and ligands used to perform the ITC experiments. All experiments were run in duplicate.

Parameters		
Total number of injections		20
Cell temperature		25 °C
Reference power		9
Initial delay		100 s
Stirring speed		850 rpm
Volume of Ist Injection		0.4 μL
Volume after Ist injection		2 μl
Injection spacing		220 s
Ligands syringe against protein (cell)	VX-809 against N-protein	100 μM against 10 μM
	Capatinib and SN 38 against N-protein	200 μM against 20 μM
	Olaparib and Paliperidine against N-protein	300 μM against 30 μM
	Darglitazone Sodium, Flibaserine, Bicuculline, and Columbianadin against N-protein	400 μM against 40 μM

2.7. Drug testing

Drug stocks were prepared in DMSO and diluted through an 8-point, 1:2 dilution series ranging from 50 μM to 0.39 μM. Vero-E6 cells were plated in 96-well plates one day prior to infection. Then cells were pre-treated with drug at a range of concentrations for 2 h and infected at multiplicity of infection (MOI) 0.05 for 1h. DMSO controls were used on every plate. In parallel, plates with only DMSO or drug (uninfected cells) were used to monitor the cytotoxicity of all the drugs. Cells were incubated with drugs at 37°C/5% CO_2 for 3 days before performing Sulphorhodamine B (SRB) assay. All treatments were performed in triplicate in each independent screen.

2.8. Plaque reduction assay

Vero-E6 cells were seeded in 24-well plates one day prior to infection. Cells were pre-treated with drug at a range of concentrations for 2 h and then infected with SARS-CoV-2 at MOI 0.1 for 24 h. Supernatant was

collected and clarified by centrifugation prior to storage at −80 °C before virus titration by plaque assay.

Confluent Vero-E6 cells in 24-well plates were washed with PBS and infected with diluted virus for 1 h. Then supernatants were removed and cells were washed with PBS before addition of 1 mL of prewarmed overlay (2% methylcellulose: propagation media containing 2% FBS = 1:2). At 48–72 h post infection, cells were fixed with 4% formaldehyde and stained with crystal violet solution after removal of the overlay, and plaques were manually quantified. The determination of all virus titers was performed in triplicate.

3. Results

3.1. Identification of multi-targeticity molecules

The identification of cost-effective multitarget SARS-CoV-2 antivirals was accomplished by structure-based virtual screening of three drug libraries: the FDA-approved drug library (Selleckchem), the NPL library (Selleckchem), and the LOPAC library (Sigma) against the following six SARS-CoV-2 target proteins: nsp12, nsp13, nsp14 CTD, nsp14 NTD, nsp15, nsp16, and N-protein. The atomic structures of all these six SARS-CoV-2 proteins contain NBPs. The top 100 compounds from each of the three libraries were selected by virtual screening. Using a SMMT approach, the binding energy for each of the molecules against all the six SARS-CoV-2 protein targets was examined. Subsequently, 30 molecules that showed binding energy equivalent or greater than the positive controls i.e., NMPs (AMP, CMP, GMP, and UMP), NTPs (ATP, CTP, GTP, and UTP), and remdesivir were selected. The molecules were then graded according to the increasing binding energies and only the top 10 compounds from the each set of library were subjected to molecular docking using the AutoDock Vina algorithm. Molecular docking binding energies of all 10 selected compounds from each of the library sets along with controls against the NBPs of SARS-CoV-2 proteins are listed in Table 3.

3.2. Computational pharmacokinetics and interaction analysis

For all the selected ligand molecules, the noted binding score was in the range of −6 kcal/mol to −12 kcal/mol. Using the bioavailability radar analysis, we further selected three drug candidates from each library using the Swiss ADME analysis tool (Daina et al., 2017). The compounds olaparib, INCB28060, and VX-809 from the FDA drug library; darglitazone sodium, paliperidone, and flibanserin from LOPAC library, and SN38, bicuculline, and columbianadin from NPL fulfilled the criteria as well as Lipinski's rule (Lipinski et al., 1997). The detailed physicochemical properties of the selected compounds are shown in Supplementary figure 1 and Supplementary Table 2. The BOILED Egg analysis has depicted the passive absorption of olaparib, INCB28060, VX-809, darglitazone sodium, paliperidone, and SN38 in the GI tract whereas bicuculline, columbianadin, and flibanserin were capable of

Table 3
Binding energies (kcal/mol) of selected ligands with SARS-CoV-2 proteins.

S.No.	Ligands	nsp12	nsp13	nsp14 NTD	nsp14 CTD	nsp15	nsp16	N
Positive Control								
1.	**AMP**	−6.8	−7.6	−6.4	−7.5	−6.5	−7.7	−5.9
2.	**CMP**	−6.0	−7.7	−5.9	−7.3	−6.3	−6.9	−5.6
3.	**GMP**	−6.8	−8.1	−6.9	−7.8	−6.7	−8.5	−6.1
4.	**UMP**	−6.2	−8.1	−6.3	−7.2	−6.3	−6.9	−5.2
5.	**ATP**	−7.3	−8.4	−6.6	−8.1	−6.1	−8.6	−6.3
6.	**CTP**	−6.4	−8.2	−6.8	−7.3	−6.2	−8.1	−5.9
7.	**GTP**	−7.2	−7.5	−7.5	−7.5	−6.4	−9.4	−6.5
8.	**UTP**	−7.3	−8.6	−6.8	−7.2	−6.5	−8.1	−5.9
9.	**Remdesivir**	−7.4	−7.3	−2.8	−9.2	−7.8	−8.0	−6.3
FDA								
1.	**Olaparib**	−8.6	−8.5	−8.7	−11.9	−8.4	−10.5	−7.7
2.	**INCB28060**	−8.6	−8.7	−8.6	−11.7	−9.3	−10.1	−7.7
3.	**VX-809**	−8.4	−8.6	−8.4	−11.2	−8.7	−10.3	−7.8
4.	**Risperidone**	−8.1	−7.8	−7.9	−9.7	−8.2	−9.9	−6.9
5.	**Ketanserin**	−8.0	−8.1	−7.1	−9.9	−7.9	−8.6	−7.3
6.	**Canagliflozin**	−8.3	−8.0	−7.4	−10.3	−7.2	−9.3	−7.3
7.	**Candesartan**	−8.1	−7.6	−7.3	−10.1	−7.6	−9.7	−6.6
8.	**PLX-4032**	−7.2	−8.4	−7.5	−11.0	−7.4	−8.9	−7.1
9.	**PLX3397**	−8.5	−7.8	−8.1	−10.2	−7.4	−9.0	−7.8
10.	**Ramatroban**	−7.3	−8.2	−7.2	−10.2	−7.9	−8.5	−6.7
LOPAC								
1.	**Darglitazone Sodium**	−8.4	−7.9	−7.6	−10.5	−8.4	−9.0	−7.0
2.	**Paliperidone**	−8.4	−8.0	−7.7	−10.8	−8.6	−10	−6.9
3.	**Flibanserin**	−7.9	−8.0	−8.2	−10.2	−8.2	−9.3	−6.9
4.	**L798106**	−7.2	−8.6	−6.2	−10.4	−7.1	−9.3	−7.5
5.	**Hydrastine**	−7.1	−7.6	−6.9	−9.7	−6.9	−9.2	−7.1
6.	**Talnetant**	−7.6	−8.0	−8.0	−9.9	−7.3	−8.2	−7.0
7.	**Droperidol**	−7.3	−7.8	−7.9	−9.3	−7.8	−8.4	−6.3
8.	**KU55933**	−7.4	−7.9	−7.8	−10.0	−7.6	−8.6	−6.0
9.	**Rutaecarpine**	−7.1	−7.9	−7.7	−9.6	−7.6	−8.4	−6.5
10.	**Psoralidin**	−7.3	−7.5	−7.5	−9.7	−8.2	−8.5	−6.5
Natural Product								
1.	**SN 38**	−8.2	−6.5	−8.6	−10.5	−8.5	−9.3	−6.8
2.	**Bicuculline**	−7.5	−9.2	−9	−10.1	−8.3	−9.7	−7.1
3.	**Columbianadin**	−7.0	−9.0	−7.5	−9.2	−7.4	−7.8	−6.8
4.	**Trilobatin**	−7.1	−7.0	−6.8	−9.4	−7.4	−8.3	−7.4
5.	**SP-146**	−9.1	−8.6	−7.2	−12.3	−9.1	−10.4	−7.3
6.	**Taxifolin-7-rhamnoside**	−8.2	−7.2	−8.4	−9.8	−7.4	−9.7	−7.0
7.	**Apigetrin**	−7.9	−7.6	−8.0	−9.9	−7.3	−8.9	−7.0
8.	**Naringin**	−9.2	−7.6	−8.3	−9.8	−7.6	−8.7	−7.1
9.	**VU6015929**	−8.1	−8.4	−6.4	−11.0	−7.5	−9.4	−6.2
10.	**Linarin**	−9.1	−7.8	−8.5	−10.7	−7.0	−9.6	−7.3

BBB penetration. In the case of effective central nervous system (CNS) acting compounds, knowledge of the drug penetration through the BBB is crucial for screening and selecting of the compounds for further assessment.

Similarly, out of nine molecules, bicuculline, columbianadin, and darglitazone sodium were predicted as Pgp^{-} (Supplementary figure 1).

The hydrogen bonds (H-bond) and hydrophobic interactions between the potential inhibitor molecules and the NBP residues of SARS-CoV-2 proteins were analysed by LIGPLOT analysis (Figs. 1–3 and Tables 4–6). The HBA and HBD interaction analysis for the protein-ligand complexes was performed, taking GMP as a reference. Based on the interaction of NMPs with the different SARS-CoV-2 proteins, GMP shows the highest binding energy (kcal/mol) as compared to other NMPs (Table 4). The comparative analysis of GMP shows that it forms the

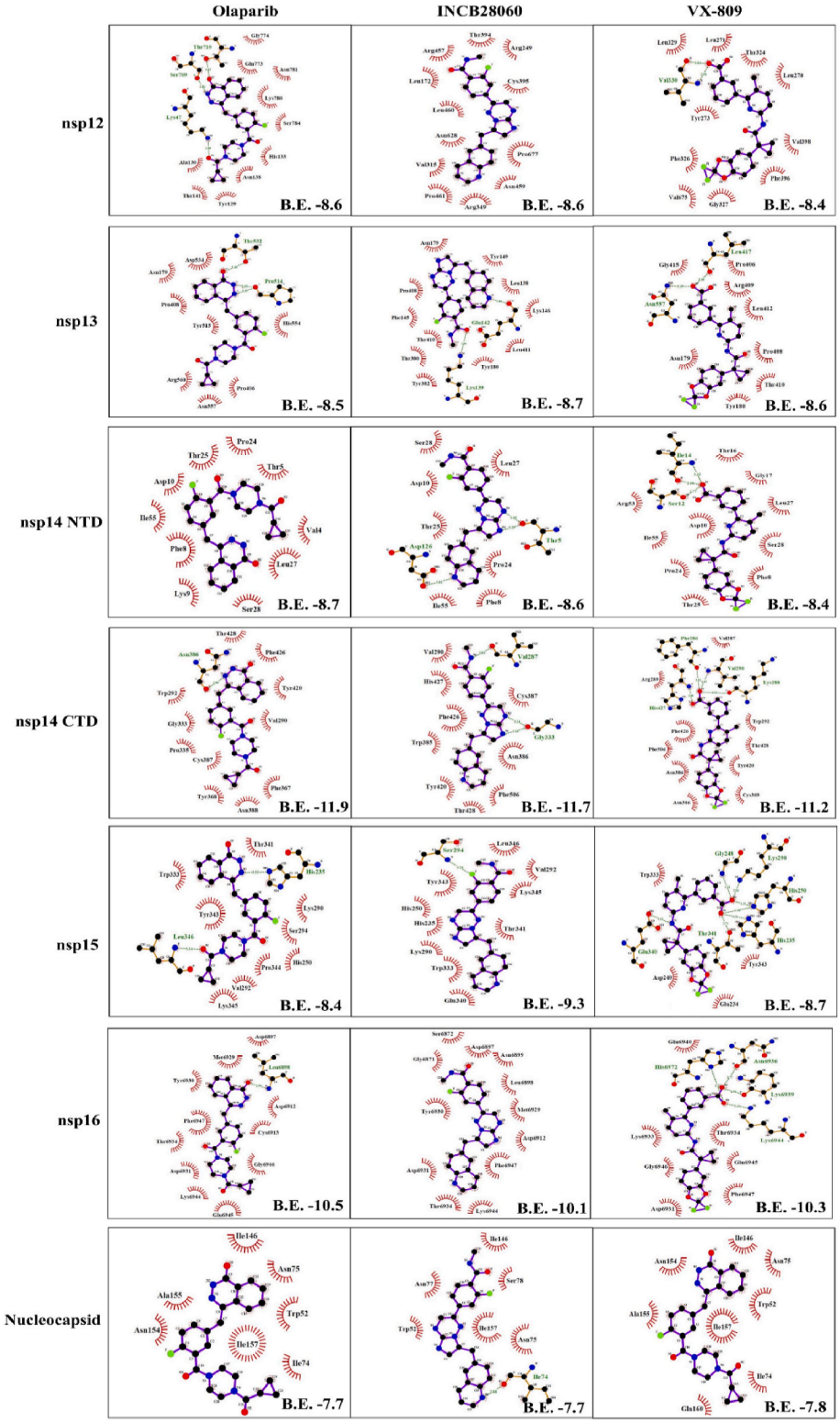

Fig. 1. Schematic presentation of selected molecules from the FDA approved drug library (Selleckchem) using the $LIGPLOT^{+}$ analysis tool.

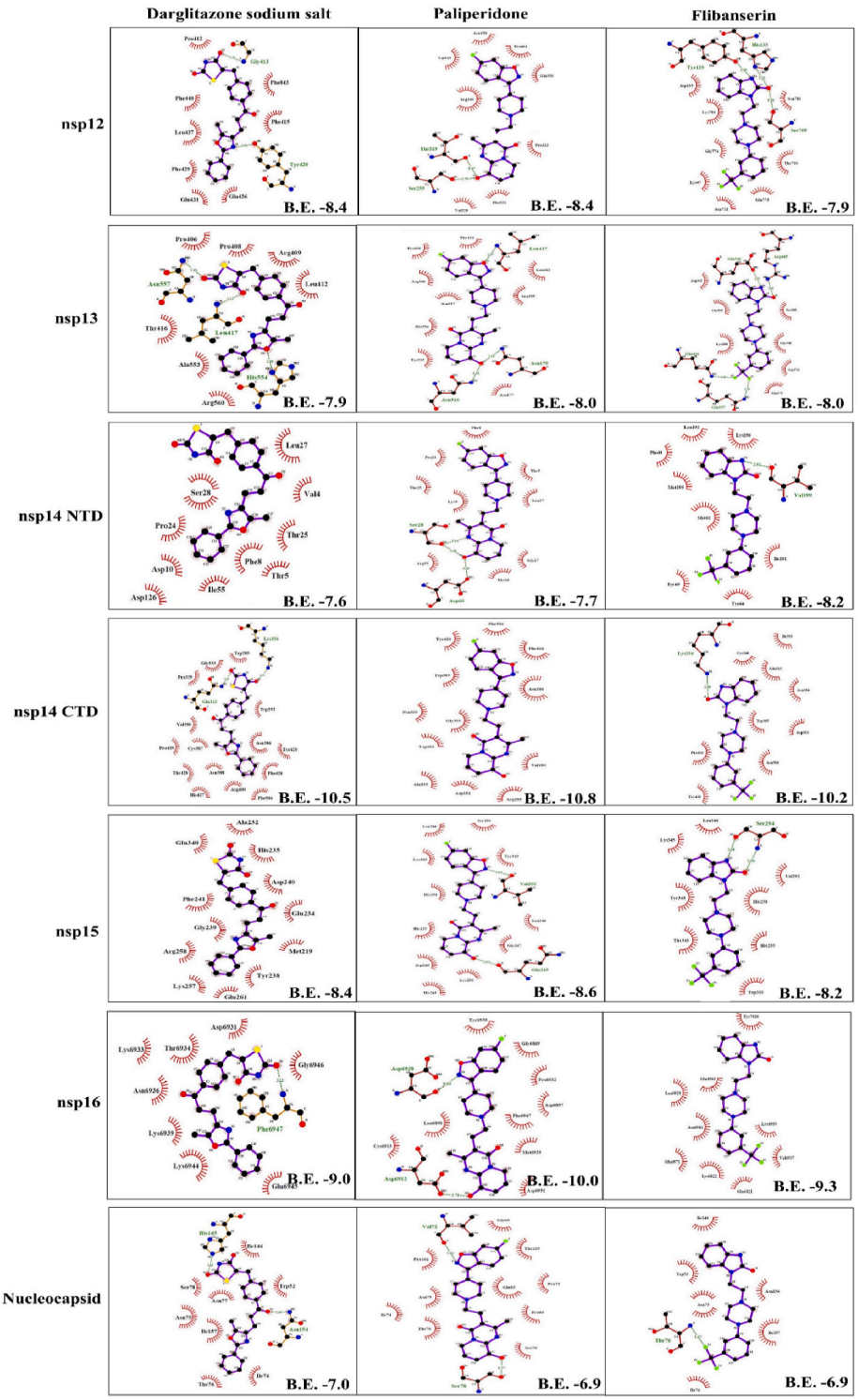

Fig. 2. Schematic presentation of selected molecules from the LOPAC drug library (Sigma) using the LIGPLOT^{+} analysis tool.

highest number of hydrogen and hydrophobic bonds with different target proteins by its HBA (N2, N5, O1, O2, O3, O4, O5, O6, O7, and O8) and HBD (N3, N4, O3, and O8) atoms. The –OH groups of the GMP have dual roles i.e., act as H-donor as well as H-acceptor (Fig. 4a). Moreover, the complete analysis of hydrogen bond and hydrophobic bond interactions in the GMP with different proteins of SARS-CoV-2 are presented in Fig. 4b. Similarly, the comparative study with inhibitor molecules has also shown the HBA and HBD groups tend to form more H-bond and hydrophobic interactions with the functional groups of the protein.

3.3. Biophysical analysis

The thermodynamic binding titration experiments were performed using ITC to validate the binding of selected compounds against the N-protein of SARS-CoV-2. The equilibrium dissociation constant (K_D), enthalpy (ΔH) and entropy ($-\Delta S$) resulting from the ITC measurements for all nine compounds are summarized in Table 7. One-site fitting

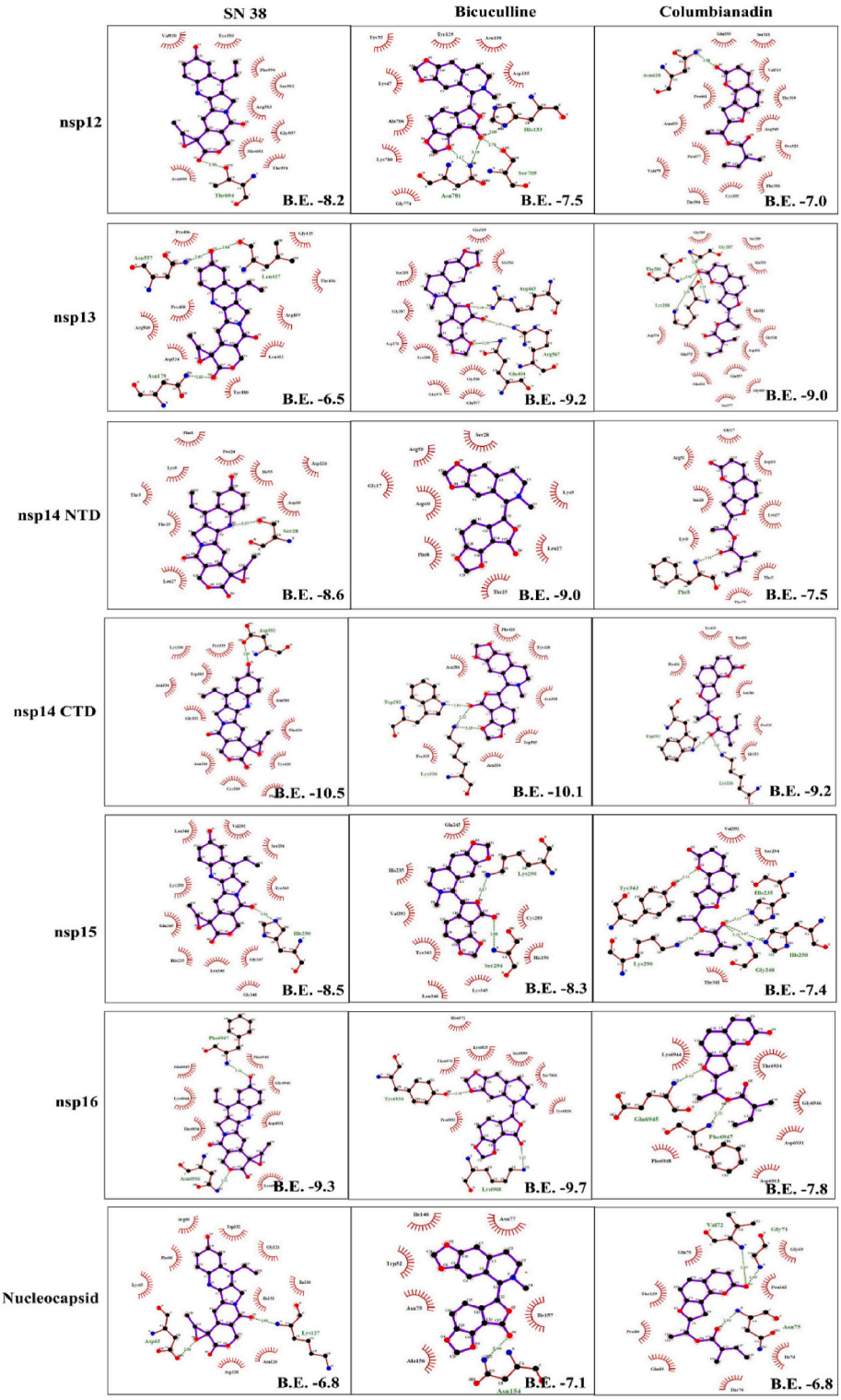

Fig. 3. Schematic presentation of selected molecules from the natural product library (Selleckchem) using the LIGPLOT^{+} analysis tool.

curves for all the selected nine compounds are shown in Fig. 5.

3.4. Antiviral assays

The antiviral activity of the top 9 screened compounds were tested against SARS-CoV-2. For each compound, the percentage cytotoxicity and inhibition were plotted and are shown in Fig. 6a and Supplementary figure 2. The three compounds: INCB28060, darglitazone sodium and columbianadin showed best antiviral activity (Fig. 6a). To validate the results, plaque reduction assays were performed. Briefly, Vero-E6 cells were pre-treated with drugs at different concentrations, followed by infection with SARS-CoV-2 at MOI 0.1 for 24 h. Supernatant was collected, clarified by centrifugation and analysed by plaque assay to determine the amount of infectious virus released. The data (Fig. 6b) show that pre-treatment of Vero-E6 cells with 50 μM INCB28060 or darglitazone sodium led to a reduction of infectious virus production of

Table 4
The H-bonds and hydrophobic interactions of selected three compounds from the FDA-drug library with the NBP of SARS-CoV-2 proteins.

Protein	Olaparib			INCB28060			VX-809		
	H bond (Å)		Hydrophobic	H bond (Å)		Hydrophobic	H bond (Å)		Hydrophobic
nsp12	Cys813 Ser814	3.06 3.17	Arg553, Asp618, Tyr619, Lys621, Asp623, Asp760, Asp761, Lys798, Trp800, Glu811, Phe812	Thr680 Thr687 Asp760	3.02 3.14 2.95	Trp617, Asp618, Tyr619, Cys622, Asp623, Ser682, Asn691, Asp761	Tyr619 Lys798 Trp800	3.24 2.99 3.05	Arg553, Trp617, Asp618, Pro620, Lys621, Asp760, Asp761, Glu811
nsp13	Ser289 Ser539	3.01 3.06	Lys288, Ala312, Ala313, Ala316, Asp374, Glu375, Arg443, Gln537, Gly538, Glu540	-		Lys288, Ser289, Ala312, Ala313, Ala316, Glu319, Asp374, Glu375, Gln537, Gly538	Lys288 Gln404 Gly538 Arg567	3.18 2.71 2.99 3.24 2.96 3.13	Pro284, Ser289, Ala312, Glu319, Arg443, Gln537, Glu540
nsp14 NTD	Asn266	3.31	Asp90, Glu92, Gly93, Asn104, Gln145, Phe146, Ala187, Phe190, Glu191, Leu253, His268, Asp273	Gly93	2.98	Val91, Glu92, Gln145, Phe146, His148, Leu149, Phe190, Leu253, Asn266, His268, Val269, Asp273	Glu92 Gly93 His148 Asp273	2.77 2.81 2.84 2.82	Asp90, Val91, Gln145, Phe146, Ala187, Phe190, Glu191, Leu253, Asn266, His268
nsp14 CTD	Asn386	2.90	Val290, Trp292, Gly333, Pro335, Phe367, Tyr368, Cys387, Asn388, Tyr420, Phe426, Thr428	Gly333 Val287	3.10 3.14 3.03	Val290, Trp385, Asn386, Cys387, Tyr420, Phe426, His427, Thr428, Phe506	Phe286 Lys288 Val290 His427	3.14 3.13 3.17 2.80	Val287, Arg289, Trp292, Asn306, Cys309, Asn386, Tyr420, Phe426, Thr428, Phe506
nsp15	His235 Leu346	3.32 3.34	His250, Lys290, Val292, Ser294, Trp333, Thr341, Tyr343, Pro344, Lys345	Ser294	3.24	His235, His250, Lys290, Val292, Trp333, Glu340, Thr341, Tyr343, Lys345, Leu346	His235 Gly248 His250 Lys290 Glu340 Thr341	3.11 3.21 3.06 3.15 2.80 3.32 2.73	Glu234, Asp240, Trp333, Tyr343
nsp16	Asn6841 Leu6898 Gly6869 Asp6928	2.75 3.02 2.80 2.82 2.93 3.30	Gly6871, Ser6872, Asp6897, Cys6913, Met6929, Tyr6930, Gly6946, Phe6947	Asn6841 Lys6844 Asp6912	3.31 3.03 3.27	Asp6897, Leu6898, Asp6928, Met6929, Tyr6930, Phe6947, Lys6968	Tyr6930	2.94	Gly6869, Gly6871, Ser6872, Asp6873, Asp6897, Leu6898, Asn6899, Cys6913, Asp6928, Met6929, Asp6931, Gly6946, Phe6947
N	Arg88 Tyr111	3.05 2.76 2.78	Ala50, Thr54, Ala55, Thr57, Ala90, Arg107, Tyr109, Arg149	Tyr111	2.81	Ala50, Ser51, Thr54, Ala55, Thr57, Ala90, Arg107, Tyr109, Arg149, Ala156	Tyr111 Arg149 Ala156	3.19 2.95 2.95 3.05	Ala50, Ser51, Thr54, Ala55, Tyr109, Ala155

Table 5
The H-bonds and hydrophobic interactions of selected three compounds from the LOPAC library with the NBP of SARS-CoV-2 proteins.

Protein	Darglitazone Sodium			Paliperidone			Flibanserin		
	H bond (Å)		Hydrophobic	H bond (Å)		Hydrophobic	H bond (Å)		Hydrophobic
nsp12	Gly413 Trp800	3.30 3.12	Tyr455, Arg553, Trp617, Asp618, Tyr619, Lys621, Cys622, Asp623, Arg624, Asp760, Asp761, Glu811	Asp761 Ser814	3.07 3.12	Arg553, Tyr619, Lys621, Cys622, Asp623, Arg624, Asp760, Glu811, Phe812, Cys813	Asp623 Trp800	2.96 3.34 3.15	Trp617, Asp618, Tyr619, Lys621, Cys622, Asp760, Asp761, Lys798
nsp13	Gly285 Lys288 Ser289 Arg443 Ser539	3.14 2.91 2.95 3.13 3.21	Pro284, Gly287, Glu375, Ala312, Ala313, Ala316, Gln537, Gly538	Gly285 Arg443	3.03 2.97	Pro284, Lys288, Ser289, Ala312, Ala313, Ala316, Ser310, Glu375, Met378, Asp534, Ser535, Gln537, Gly538	Gly287 Lys288	3.23 2.87 3.25	Gly285, Ala312, Ala313, Ala316, Glu375, Arg443, Gln537, Gly538, Glu540
nsp14 NTD	Gly93 Asn104	3.17 2.97	Asp90, Val91, Glu92, Gln145, Phe146, His148, Trp186, Phe190, Leu253, Asn266, His268, Val269, Ala270, Asp273	Gln145 His268	3.18 2.93	Asp90, Glu92, Gly93, Asn104, Phe146, Phe190, Glu191, Leu253, Asn266, Asp273	His148 Ala187 Glu191	3.33 2.92 3.14 2.81	Asp90, Glu92, Gln145, Phe146, Trp186, Phe190, Asn266, His268, Asp273
nsp14 CTD	Gln313 Lys336	2.96 2.94	Val290, Trp292, Gly333, Pro335, Trp385, Asn386, Cys387, Asn388, Arg400, Tyr420, Phe426, His427, Thr428, Pro429, Phe506	-		Arg289, Val290, Trp292, Gly333, Pro335, Asp352, Ala353, Trp385, Asn386, Tyr420, Phe426, Phe506,	Lys336	2.99	Gln313, Asp331, Asn334, Ile338, Cys340, Trp385, Asn386, Tyr420, Phe426
nsp15	–		Met219, Ala232, Glu234, His235, Tyr238, Gly239, Asp240, Phe241, Arg258, Lys257, Glu261, Glu340	Glu245 Val292	2.93 3.04	His235, Asp240, Leu246, Gly247, His243, His250, Lys290, Ser294, Tyr343, Lys345, Leu346	Ser294	2.81 3.06	His235, His250, Val292, Trp333, Thr341, Tyr343, Lys345, Leu346
nsp16	Asp6873 Tyr6930 Lys6968 Asn6996	3.08 2.93 3.06 3.09	Asn6841, Lys6844, Gly6871, Ser6872, Asp6897, Leu6898, Asp6928, Met6929, Phe6947, Glu7001	Asp6912 Asp6928	2.70 2.85	Gly6869, Asp6897, Leu6898, Met6929, Tyr6930, Cys6913, Tyr6930, Asp6931, Phe6947	Lys6968	3.05	Gly6869, Gly6871, Asp6897, Leu6898, Asp6912, Cys6913, Asp6928, Met6929, Tyr6930, Pro6932, Phe6947
N	Arg107 Arg149	3.23 3.20	Thr54, Ala55, Thr57, Tyr109, Tyr111, Ala156	Tyr111	2.71	Ala50, Thr54, Ala55, Ala90, Arg107, Tyr109, Arg149, Ala156	Ser51 Ala55	2.89 3.08	Thr54, Tyr109, Tyr111, Arg149, Ala173

Table 6
The H-bonds and hydrophobic interactions of selected three compounds from the Natural Product library with the NBP of SARS-CoV-2 proteins.

Protein	SN 38			Bicuculline			Columbianadin		
	H bond (Å)		Hydrophobic	H bond (Å)		Hydrophobic	H bond (Å)		Hydrophobic
nsp12	Asp618 Arg624	2.99 3.08 3.22	Arg553, Tyr619, Pro620, Lys621, Asp623, Lys798	Asn691	2.91	Arg553, Tyr619, Lys621, Cys622, Asp623, Arg624, Ser759, Asp760	Thr556 Arg624	3.21 3.08	Tyr455, Arg553, Arg555, Tyr619, Lys621, Asp623, Ser682
nsp13	Glu375	3.21	Lys288, Ser289, Ala316, Asp374, Gly538	Gln404 Arg443 Arg567	2.93 2.74 3.07	Lys288, Ser289, Ala316, Asp374, Glu375, Gln537, Gly538	Thr286 Gly287 Lys288	2.95 2.94 3.17 3.19	Gly285, Ser289, Ala313, Ala316, Glu375, Ser377, Gly400, Asp401, Gln404, Gln537, Gly538
nsp14 NTD	Gly93	2.62	Asp90, Glu92, Asn104, Pro141, Gln145, Phe146, Trp186, Phe190, Leu253, Gln254, Asp273	Asp90 Gly93	3.16 3.07	Val91, Glu92, Asn104, Gln145, Trp186, Ala187, Phe190, Glu191, Leu253, Asp273	Asn266	2.94	Asp90, Val91, Glu92, Gln145, Phe146, Phe190, Glu191, Leu253, His268, Val269, Asp273
nsp14 CTD	Asp352	2.89	Trp292, Asn306, Cys309, Gly333, Asn334, Pro335, Lys336, Asn386, Tyr420, Phe426, Phe506	Trp292 Lys336	3.03 3.19 3.22	Asn306, Asn334, Pro335, Trp385, Asn386, Tyr420, Phe426	Trp292 Lys336	3.18 3.02	Gly333, Pro335, Asp386, Tyr420, Phe426, Thr428
nsp15	His250	3.16	His235, Gln245, Leu246, Gly247, Gly248, Lys290, Val292, Ser294, Tyr343, Leu346	Lys290 Ser294	3.17 2.88	His235, Gln245, His250, Val292, Cys293, Tyr343, Lys345, Leu346	His235 Gly248 His250 Lys290 Tyr343	3.17 3.12 3.07 2.98 3.11	Val292, Ser294, Thr341
nsp16	Cys6913	2.87 3.32	Gly6871, Ser6872, Asp6873, Asp6897, Leu6898, Asp6912, Met6929, Tyr6930, Asp6931, Pro6932,	Asn6899	2.99	Asp6897, Leu6898, Asp6912, Cys6913, Asp6928, Met6929, Tyr6930, Asp6931, Phe6947	Asn6899 Phe6947	2.90 3.12	Gly6869, Asp6897, Leu6898, Asp6912, Asp6928, Met6929, Tyr6930, Asp6931, Phe6947
N	Thr57 Arg107 Arg149 Ala173	2.91 3.03 3.31 2.96	Thr54, Ala55, Tyr109, Ala155, Ala156	Ser51 Arg149	2.80 2.96	Ala50, Thr54, Ala55, Arg107, Tyr109, Tyr111, Pro151	Arg107 Arg149 Asn75	3.15 3.09 2.81	Ala50, Ser51, Phe53, Thr54, Ala90, Tyr109, Tyr111, Pro151, Ala156

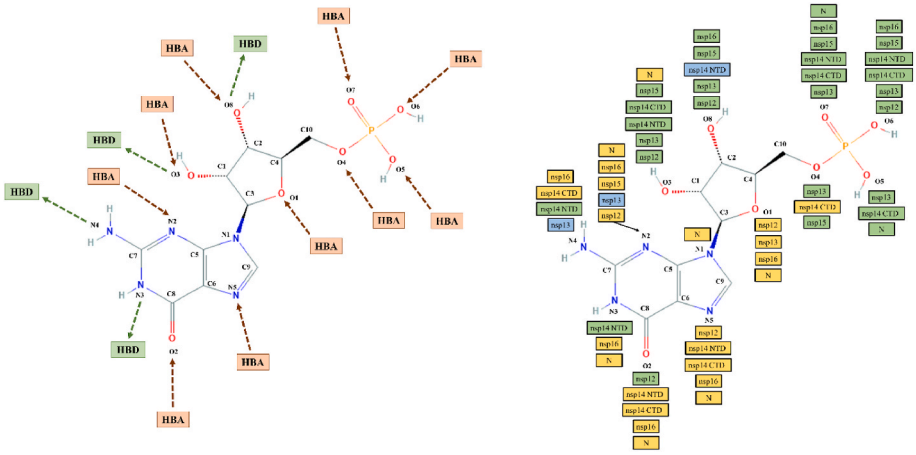

Fig. 4. (a) Representation of H-bond acceptor (HBA; shown in the red box) and H-bond donor (HBD; shown in the green box) in the GMP molecule. (b) Representation of H bond and hydrophobic interactions of HBA and HBD of GMP molecule with different SARS-CoV-2 proteins. The green box shows both hydrogen and hydrophobic interactions, the yellow box shows only hydrophobic interactions, and the blue box shows only hydrogen bonds.

over 3 orders of magnitude, confirming antiviral efficiency of these compounds.

4. Discussion

SARS-CoV-2, the etiological agent of COVID-19, has caused a global pandemic that has hugely disrupted social and economic life. The ever-increasing number of SARS-CoV-2 variants have raised serious health concerns for humans. Its high transmission, recombination and mortality rates have had tragic consequences around the world. Genetic variability in SARS-CoV-2 genome is a result of random mutations and/or recombination that can alter amino acids and viral phenotype. Few mutants gets naturally selected due to its increased fitness for viral replication, transmission and/or ability to evade the host immunity, leading to the emergence of new strains (Gribble et al., 2021; Safari and Elahi, 2022). The emergence of new strains of SARS-CoV-2 are pressurizing the scientific community to investigate small molecule-based therapeutics to combat the emerging viral pathogens.

In this regard, the NBPs of viral enzymes and proteins are promising targets in the quest for effective antiviral molecules. Because nucleosides/nucleotides are the building blocks of RNA and DNA, slight variations to the nucleoside scaffold can have perilous implications. Many virus-specific proteins contain these NBPs such as RdRp, helicase, MTase, nucleocapsid, etc., and these have been targeted in this study. The FDA has authorized several antiviral nucleoside/nucleotide analog drugs targeting different viruses, such as idoxuridine, which was approved by the FDA in 1962 against HSV. It mimics thymidine and, once incorporated into the nascent viral genome during replication, blocks chain elongation (Wilhelmus, 2015). Ribavirin was approved for the treatment of severe respiratory syncytial virus (RSV) infection

Table 7
The thermodynamic analysis of top hit compounds with N-protein of SARS-CoV-2 protein as obtained from ITC. n = stoichiometry, K_A = association constant, K_D= equilibrium dissociation constant, ΔH= enthalpy, ΔS= entropy.

Ligands	n	K_D (μM)	$K_A(M^{-1})$	ΔH (cal/mol)	ΔS (cal/mol/degree)
Olaparib	1	66.2	$(1.51)10^4 \pm 905$	$(-1.68)10^5 \pm 6083$	−545
INCB28060	1	331	$(3.02)10^3 \pm 132$	$(-4.015)10^6 \pm (1.7)10^5$	$(-1.34)10^4$
VX-809	1	54.3	$(1.84)10^4 \pm 507$	$(-7.71)10^6 \pm (1.6)10^5$	$(-2.58)10^4$
Darglitazone Sodium	1	72	$(1.38)10^4 \pm 635$	$(-1.487)10^5 \pm 3840$	−480
Paliperidone	1	234	$(4.26)10^3 \pm 110$	$(-2.55)10^5 \pm 4873$	−838
Flibaserine	1	352	$(2.84)10^3 \pm 216$	$(-2.47)10^5 \pm (1.5)10^4$	−815
SN 38	1	40	$(2.46)10^4 \pm (4.33)10^3$	$(-1.38)10^5 \pm (1.43)10^4$	−444
Bicuculline	1	92	$(1.08)10^4 \pm 414$	$(-1.667)10^5 \pm 3874$	−540
Columbianadin	1	854	$(1.17)10^4 \pm 112$	$(-1.851)10^5 \pm (1.51)10^4$	−607

(Pelaez et al., 2009), Lassa fever virus infection (Eberhardt et al., 2019), and influenza A and B virus infections (Smee et al., 2006). But now, it has been approved for use against HBV and HCV (Liu et al., 2003) and also for many other viruses including coronaviruses (Eslami et al., 2020; Simonis et al., 2021). These medications are nucleotide derivatives that compete with the physiological nucleotides for binding to the NBPs of the viral proteins.

The use of *in silico* methods in drug discovery has increased dramatically in recent years. Such methods can provide firm evidence for the evaluation of any drug molecule by its interaction with the target protein and its bioavailability inside the host organism. The multi-proteins targeting approach in this study has identified drug molecules that could be tested *in vivo* for efficacy and further drug development. Furthermore, considering the high likelihood that this will not be the last pandemic we face, as the other infectious viral diseases are circulating worldwide. It is critical that we develop these strategies to combat the other viral diseases such as chikungunya and dengue fevers, for which till date there are no antivirals available in the market (Aggarwal et al., 2017; Mudgal et al., 2020; Pareek et al., 2022; Sharma et al., 2018, 2016; Singh et al., 2018).

The aim of these computational studies was two-fold. First, a more precise assessment of the Vina scores (binding energy in kcal/mol) against the NBPs and another is the quest for the single ligand aimed at targeting the multi-protein of SARS-CoV-2. Although the identification of drug molecules from *in silico* methods have been proved as a beneficial practice, studies of the *in vivo* behaviour of those compounds have been a bottleneck. The drug-likeness of any compound can be proven when it possesses the right balance between its molecular properties and structural features. The SwissADME online server estimates the drug-likeness of compounds by predicting their Absorption, Distribution, Metabolism, and Excretion (ADME) properties. This method is an efficient alternative approach to evade the time wastage by drug molecules due to their toxicity and cell membrane permeability.

The virtual screening of three different libraries with different proteins of SARS-CoV-2 has resulted in the top 100 potential antiviral compounds. For many compounds, the binding energy was very high i.e., in the range of −6 kcal/mol to −12 kcal/mol. Further, we have selected the top 30 compounds whose binding energy was equal or greater than positive control in the selected set of the SARS-CoV-2 proteins. Out of 30 compounds, we further shortlisted the best 10 compounds from each set of the library. NMPs, NTPs, and remdesivir were used as a positive control, as NMPs is the one that generally binds to the nucleotide binding site, while remdesivir is already a well-established drug compound in the research area against many RNA viruses like SARS-CoV-2, MERS-CoV, SARS-CoV, Ebola virus, and others (Malin et al., 2021; Simonis et al., 2021). The final binding energy was obtained after molecular docking of all the compounds. The antiviral potency of a drug candidate is rather incomplete until it is unable to act well in *in vivo* conditions.

Further, the drug-likeness of the top 10 compounds from each compound library were predicted. These compounds had high binding energies for the viral targets but the physicochemical parameters for the drug-likeness of most of these molecules did not show acceptable properties. The physiochemical properties of compounds define the kinetics of drug exposure to the tissue and thus affect their pharmacological activities. After the molecular docking of the selected compounds, these were further evaluated using the thermodynamic criteria. Supplementary Table 2 shows the performance and the pharmacological activity of the best-selected compounds in each set of the library. A compound usually follows the Lipinski rule of five for the better efficacy of the therapeutic molecules. The bioavailability radar of SwissADME also follows other metric algorithms for the calculation of the pharmacological kinetics of the compounds. A compound is expected to have high absorption when the size of the compound is < 500 kDa, the n-octanol to water partition coefficient (log P) is < 5, the number of H bond donor and acceptor is < 5 and < 10 respectively, and the molar refractivity index is in the range of 40–130. Based on these pharmacological properties of compounds, only top 3 best compounds were obtained from each set of the library (olaparib, INCB28060, and VX-809 from FDA; darglitazone sodium, paliperidone, and flibanserin from LOPAC; SN 38, bicuculline, and columbianadin from Natural Product libraries) that show the antiviral potential against this pandemic virus. These compounds are already has been used as anti-cancer and anti-inflammatory agents, among other uses (Table 8).

Bioavailability radar including the BOILED egg pictorial representation is provided in the Supplementary figures 1. The best nine selected compounds were shortlisted as potential drug molecules. The molecules which have been depicted as Pgp + can be engineered by increasing steric hindrance to HBD, decreasing the HBA potential, impeding Pgp binding, and decreasing bilayer penetration for their better absorption and effectivity. Afterward, the LIGPLOT analysis of these compounds has been studied for the schematic presentation of the interaction between the ligand-protein complexes. (Tables 4–6, Figs. 1–3). Interestingly, among the H-bond and hydrophobic interactions of all the proteins, we have found that all nine promising compounds (three from each library) mostly share similar interacting amino acids (Table 9).

In the HBD, a hydrogen atom is bonded to nitrogen, oxygen, and sulfur (strong electronegative atoms) while in HBA, the nitrogen and oxygen atoms are in double and triple bonds, which contains lone pair. The HBA and HBD of protein-ligand complexes only form when the interaction between ligand and water molecule dissociates (Wilkinson et al., 1984). The comparative LIGPLOT analysis shows the importance of both HBA and HBD in the molecules to qualify as a drug. More HBA and HBD in the protein-ligand complexes can lead to better interaction during the administration and can have a prolonged drug effect in *in vitro* and *in vivo* studies (Zheng et al., 2017). For the improved drug-target interactions, either the modifications are made in the drug or target molecule, or their interaction interface is engineered (Varma et al., 2010). So here, we predicted that probable modification by conformational favorable functional groups in identified molecules could lead to enhanced stability and binding affinity of protein-ligand complexes.

The thermodynamic parameter and binding affinities of the most promising compounds were further experimentally assessed using ITC. ITC analysis yielded K_D values in the range of 40–854 μM that positively shows the molecular interaction with the compounds (Table 7). The strength of the binding affinities between the protein and a compound can be assessed by the K_D value (Krainer et al., 2012). Thus, the

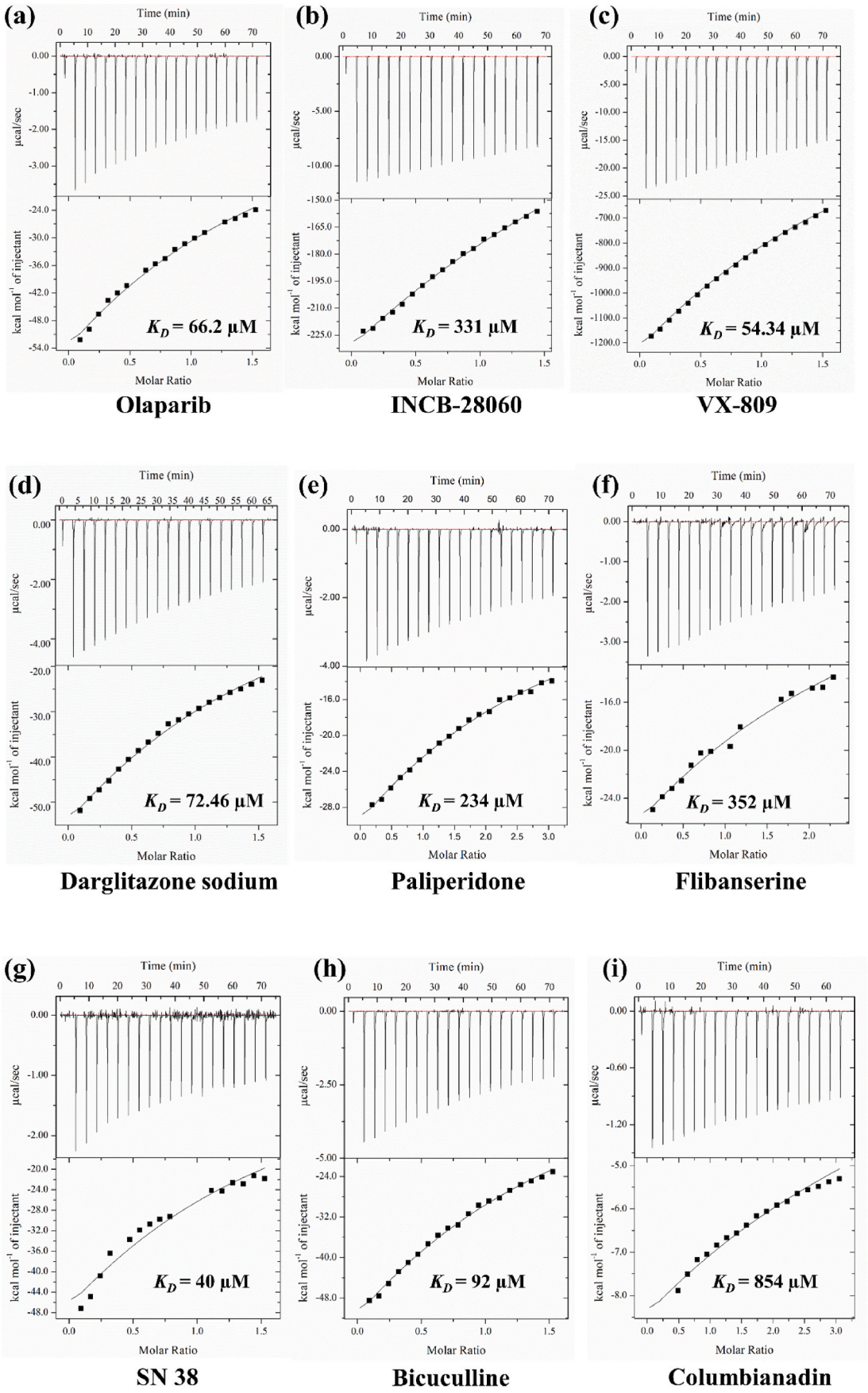

Fig. 5. Binding isotherms of identified compounds using ITC: Thermodynamic profiles of ligands (a) Olaparib, (b) INCB28060, (c) VX-809, (d) Darglitazone Sodium, (e) Paliperidone, (f) Flibaserine, (g) SN 38, (h) Bicuculline, (i) Columbianadin, against the purified SARS-CoV-2 N-protein.

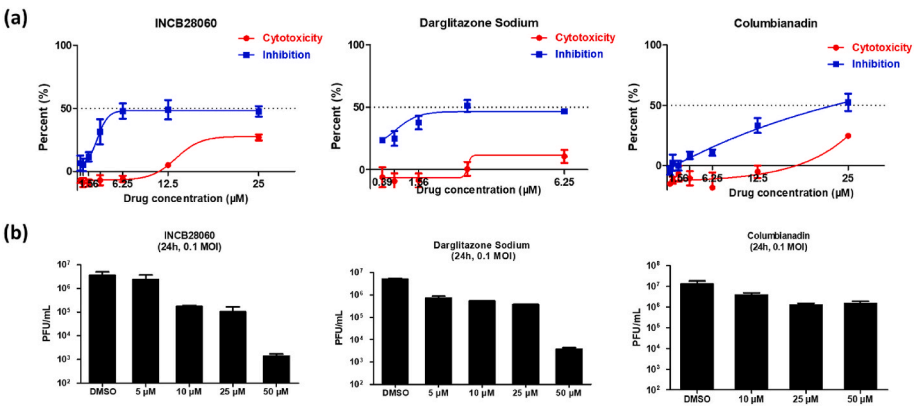

Fig. 6. Antiviral screening for drugs targeting SARS-CoV-2 (a) Percent cytotoxicity and percent inhibition graphs from drug screens. Triplicate wells of Vero-E6 cells were pre-treated with the indicated drugs for 2 h prior to infection with SARS-CoV-2 at MOI 0.05. Cells were incubated for 72 h prior to performing SRB assay. Cytotoxicity data was normalized according to cell only (DMSO) controls and DMEM media only (blank) controls. Inhibition data was normalized to the cell only (DMSO) controls and the infected controls (DMSO treated and infected cells). (b) INCB28060, darglitazone sodium and columbiandin inhibit production of SARS-CoV-2. Vero-E6 cells were pre-treated with indicated concentrations of drugs for 2 h prior to infection with SARS-CoV-2 at MOI 0.1 and harvested supernatant at 24 h post-infection (hpi) for plaque assay.

Table 8
Functions of identified potential drug compounds.

Ligands	Functions	Reference
FDA		
Olaparib	Inhibits poly (ADP-ribose) polymerase (PARP) and antitumor effects with BRCA1 or BRCA2 mutations against breast cancer and ovarian cancer.	(Fong et al., 2009; Moore et al., 2018; Robson et al., 2017)
VX-809	In phase 3 trial with ivacaftor, which contains corrector and potentiator for treatment of cystic fibrosis.	(Deeks, 2016; Ratjen et al., 2017)
INCB28060	Anti-neoplastic and anti-cancerous actions. It is orally available as a mesenchymal-epithelial transition (MET) inhibitor for the treatment of lung cancer.	(Dhillon, 2020; Vansteenkiste et al., 2019)
LOPAC		
Darglitazone Sodium	Increases CD36 mRNA levels and protein expression in human macrophage cells. Controls blood glucose levels in the treatment of non-insulin-dependent diabetes mellitus (NIDDM).	(Chaiken et al., 1995; Svensson et al., 2003)
Flibanserin	Clinically approved drug for hypoactive sexual desire disorder (HSDD) in women by modifying neurotransmitters.	(Shapiro et al., 2017; Vallejos and Wu, 2017)
Paliperidone	For the treatment of schizoaffective disorder (SCA) and works as a mood stabilizer by acting at the prefrontal cortex.	(Alphs et al., 2016; Corena-McLeod, 2015)
Natural Product		
SN 38	Anti-proliferative and anti-tumor roles by activating MAPK pathways and boosting IL-8 expression.	(Bi et al., 2018; Zhang et al., 2017)
Bicuculline	The antagonist of receptors of inhibitory neurotransmitter GABA and enhances calcium secretion.	(Johnston, 2013; Mestdagh and Wülfert, 1999)
Columbianadin	Anti-cancerous and anti-inflammatory effects by inducing necroptosis and apoptosis. Inhibits nociceptive pain behaviours by inhibiting calcium channels in neurons.	(Kang et al., 2016; Su et al., 2019)

biophysical characterization of these selected molecules confirmed the binding to the N-protein.

While, in *in vitro* assays, we found that 3 of 9 potential compounds (INCB28060, Darglitazone Sodium and Columbianadin) display substantial antiviral activity in different *in vitro* assays (Fig. 6 and Supplementary figure 2). Darglitazone Sodium, the most effective compound, has an EC_{50} value under 10 μM (Supplementary Table 3). The three drug candidates were further tested for antiviral activity at the level of inhibiting viral particle production. All three drugs showed inhibitory properties, but INCB28060 and Darglitazone Sodium had greater anti-SARS-CoV-2 activity (Fig. 6). Interestingly, Columbianadin identified as potential antiviral molecule against SARS-CoV-2, is reported as a bioactive compound that has analgesic, anti-inflammatory, antitumor property, and inhibitor of voltage-gated Ca^{2+} channels (Chen et al., 1995; Kang et al., 2016; Su et al., 2019). The ion channels are being investigated as therapeutic targets for various viral diseases including SARS-CoV-2 (Charlton et al., 2020; Navarese et al., 2020; Ou et al., 2020). Therefore, the antiviral effect of Columbianadin against SARS-CoV-2 may also be due to the modulation of the ion channel activity, and requires further detailed experimental investigations.

5. Conclusions

In summary, structure-based virtual screening, molecular docking, molecular repurposing, ADME analysis, biophysical studies and *in vitro* cell-based testing have fulfilled the main objective of the approach to finding a potential single drug molecule that targets multiple proteins of SARS-CoV-2. These identified drug molecules have already undergone clinical and research stages for other medical interventions, and therefore, repurposing of these compounds for antiviral therapy against SARS-CoV-2 is anticipated.

CRediT authorship contribution statement

Ruchi Rani: Conceptualization, Data curation, Formal analysis, Investigation, Methodology, Validation, Visualization, Writing – original draft, Writing – review & editing. **Siwen Long:** Conceptualization, Data curation, Formal analysis, Investigation, Methodology, Validation, Visualization, Writing – original draft, Writing – review & editing. **Akshay Pareek:** Conceptualization, Data curation, Investigation, Methodology, Validation, Visualization, Writing – original draft. **Preeti Dhaka:** Data curation, Investigation, Validation, Visualization, Writing – original draft, Writing – review & editing. **Ankur Singh:** Data curation, Validation, Visualization, Writing – review & editing. **Pravindra Kumar:** Conceptualization, Data curation, Formal analysis, Funding acquisition, Investigation, Methodology, Resources, Supervision, Validation, Writing – review & editing. **Gerald McInerney:** Conceptualization, Data curation, Formal analysis, Funding acquisition, Investigation, Methodology, Resources, Supervision, Validation, Writing – review & editing. **Shailly Tomar:** Data curation, Investigation, Methodology, Supervision, Validation, Writing – review & editing.

Declaration of competing interest

The authors declare that they have no known competing financial

Table 9
Common interacting residues between different SARS-CoV-2 proteins and drug libraries.

	nsp12	nsp13	nsp14 NTD	nsp14 CTD	nsp15	nsp16	N
FDA	Asp618, Asp760, Asp761, Tyr619	Lys288, Ser289, Ala312, Glu537, Gly538	Gly93, Gln145, Phe146, Phe190, Leu253, His268, Asp273	Tyr420, Phe426, Thr428	His250, Lys290, Trp333, Thr341, Tyr343	Met6929, Phe6947, Tyr6930	Ala50, Thr54, Ala55, Tyr109, Tyr111, Arg149
LOPAC	Tyr619, Lys621, Cys622, Asp623, Asp760, Asp761	Gly285, Lys288, Ala312, Ala313, Ala316, Glu537, Gly538	Asp90, Glu92, Gln145	Trp385, Asn386, Tyr420, Phe426	His235, His250	Asp6897, Leu6898, Asp6928, Met6929, Tyr6930, Phe6947	Thr54, Ala55, Tyr109, Arg149
NPL	Arg553, Lys621, Asp623, Arg624	Lys288, Ser289, Ala316, Gly538	Asp90, Glu92, Gln145, Phe190, Leu253, Asp273	Trp292 Pro335, Asp386, Tyr420, Phe426	Val292, Ser294, His235, His250, Lys290, Tyr343	Asp6897, Leu6898, Asp6912, Met6929, Tyr6930, Asp6931	Thr54, Arg107, Tyr109, Arg149

interests or personal relationships that could have appeared to influence the work reported in this paper.

Acknowledgments

The authors are thankful to Department of Biosciences and Bioengineering, IIT Roorkee for computational facilities. RR and AP would like to thank University Grants Commission (UGC) and Council of Scientific and Industrial Research (CSIR) for providing financial support. ST and PK acknowledges and thanks Intensification of Research in High Priority Areas (IRHPA) program of Science and Engineering Research Board (SERB), Department of Science & Technology (DST), Government of India for supporting this study (Grant No.- IPA/2020/000054). SL was supported by a stipend from the China Scholarship Council (CSC). Work in the GM laboratory is supported by project grants from the Swedish Research Council (Vetenskapsrådet) (2018-03914 and 2020-04706).

Appendix A. Supplementary data

Supplementary data to this article can be found online at https://doi.org/10.1016/j.virol.2022.08.008.

References

Aggarwal, M., Kaur, R., Saha, A., Mudgal, R., Yadav, R., Dash, P.K., Parida, M., Kumar, P., Tomar, S., 2017. Evaluation of antiviral activity of piperazine against Chikungunya virus targeting hydrophobic pocket of alphavirus capsid protein. Antivir. Res. 146, 102–111. https://doi.org/10.1016/j.antiviral.2017.08.015.

Ali, F., Kasry, A., Amin, M., 2021. The new SARS-CoV-2 strain shows a stronger binding affinity to ACE2 due to N501Y mutant. Med. Drug Discov. 10 https://doi.org/10.1016/j.medidd.2021.100086.

Alphs, L., Fu, D.J., Turkoz, I., 2016. Paliperidone for the treatment of schizoaffective disorder. Expet Opin. Pharmacother. 17, 871–883. https://doi.org/10.1517/14656566.2016.1161029.

Anderson, P.L., Rower, J.E., 2010. Zidovudine and lamivudine for HIV infection. Clin. Med. Rev. Therapeut. 2, 115–127. https://doi.org/10.4137/cmrt.s4557.

Árquez, M.A., Martín-Alonso, S., Gorelick, R.J., Scott, W.A., Acosta-Hoyos, A.J., Menéndez-Arias, L., 2020. Nucleocapsid protein precursors NCp9 and NCp15 suppress ATP-mediated rescue of AZT-terminated primers by HIV-1 reverse transcriptase. Antimicrob. Agents Chemother. 64 https://doi.org/10.1128/AAC.00958-20.

Berman, H.M., Westbrook, J., Feng, Z., Gilliland, G., Bhat, T.N., Weissig, H., Shindyalov, I.N., Bourne, P.E., 2000. The protein Data Bank. Nucleic Acids Res. https://doi.org/10.1093/nar/28.1.235.

Bi, Y., Lee, R.J., Wang, X., Sun, Y., Wang, M., Li, L., Li, C., Xie, J., Teng, L., 2018. Liposomal codelivery of an SN38 prodrug and a survivin siRNA for tumor therapy. Int. J. Nanomed. 13, 5811–5822. https://doi.org/10.2147/IJN.S173279.

Chaiken, R.L., Eckert-Norton, M., Pasmantier, R., Boden, G., Ryan, I., Gelfand, R.A., Lebovitz, H.E., 1995. Metabolic effects of darglitazone, an insulin sensitizer, in NIDDM subjects. Diabetologia 38, 1307–1312. https://doi.org/10.1007/BF00401763.

Chan, J.F.W., Kok, K.H., Zhu, Z., Chu, H., To, K.K.W., Yuan, S., Yuen, K.Y., 2020. Genomic characterization of the 2019 novel human-pathogenic coronavirus isolated from a patient with atypical pneumonia after visiting Wuhan. Emerg. Microb. Infect. 9, 221–236. https://doi.org/10.1080/22221751.2020.1719902.

Chang, C.K., Hou, M.H., Chang, C.F., Hsiao, C.D., Huang, T.H., 2014. The SARS coronavirus nucleocapsid protein - forms and functions. Antivir. Res. https://doi.org/10.1016/j.antiviral.2013.12.009.

Charlton, F.W., Pearson, H.M., Hover, S., Lippiat, J.D., Fontana, J., Barr, J.N., Mankouri, J., 2020. Ion Channels as therapeutic targets for viral infections: further discoveries and future perspectives. Viruses. https://doi.org/10.3390/v12080844.

Chen, Y.F., Tsai, H.Y., Wu, T.S., 1995. Anti-inflammatory and analgesic activities from roots of Angelica pubescens. Planta Med. 61, 2–8. https://doi.org/10.1055/s-2006-957987.

Corena-McLeod, M., 2015. Comparative Pharmacology of Risperidone and Paliperidone. Drugs R D. https://doi.org/10.1007/s40268-015-0092-x.

Daina, A., Zoete, V., 2016. A BOILED-egg to predict gastrointestinal absorption and brain penetration of small molecules. ChemMedChem 11, 1117–1121. https://doi.org/10.1002/cmdc.201600182.

Daina, A., Michielin, O., Zoete, V., 2017. SwissADME: a free web tool to evaluate pharmacokinetics, drug-likeness and medicinal chemistry friendliness of small molecules. Sci. Rep. 7, 1–13. https://doi.org/10.1038/srep42717.

Dallakyan, S., Olson, A.J., 2015. Small-molecule library screening by docking with PyRx. Methods Mol. Biol. 1263, 243–250. https://doi.org/10.1007/978-1-4939-2269-7_19.

de Groot, R.J., Baker, S.C., Baric, R.S., Brown, C.S., Drosten, C., Enjuanes, L., Fouchier, R. A.M., Galiano, M., Gorbalenya, A.E., Memish, Z.A., Perlman, S., Poon, L.L.M., Snijder, E.J., Stephens, G.M., Woo, P.C.Y., Zaki, A.M., Zambon, M., Ziebuhr, J., 2013. Commentary: Middle East respiratory syndrome coronavirus (MERS-CoV): announcement of the coronavirus study group. J. Virol. 87, 7790–7792. https://doi.org/10.1128/jvi.01244-13.

Deeks, E.D., 2016. Lumacaftor/Ivacaftor: a review in cystic fibrosis. Drugs 76, 1191–1201. https://doi.org/10.1007/s40265-016-0611-2.

Dhaka, P., Singh, A., Choudhary, S., Kumar, P., Kumar Sharma, G., Tomar, S., Gaurav, *, Sharma, K., 2022. Discovery of Anti-SARS-CoV-2 Molecules Using Structure-Assisted Repurposing Approach Targeting N-Protein. bioRxiv. https://doi.org/10.1101/2022.03.12.484092, 2022 03.12.484092.

Dhillon, S., 2020. Capmatinib: first approval. Drugs 80, 1125–1131. https://doi.org/10.1007/s40265-020-01347-3.

Dimou, E., Papadimitropoulos, V., Hadziyannis, S.J., 2007. The role of entecavir in the treatment of chronic hepatitis B. Therapeut. Clin. Risk Manag.

Drexler, J.F., Corman, V.M., Drosten, C., 2014. Ecology, evolution and classification of bat coronaviruses in the aftermath of SARS. Antivir. Res. https://doi.org/10.1016/j.antiviral.2013.10.013.

Eberhardt, K.A., Mischlinger, J., Jordan, S., Groger, M., Günther, S., Ramharter, M., 2019. Ribavirin for the treatment of Lassa fever: a systematic review and meta-analysis. Int. J. Infect. Dis. https://doi.org/10.1016/j.ijid.2019.07.015.

Eslami, G., Mousaviasl, S., Radmanesh, E., Jelvay, S., Bitaraf, S., Simmons, B., Wentzel, H., Hill, A., Sadeghi, A., Freeman, J., Salmanzadeh, S., Esmaeilian, H., Mobarak, M., Tabibi, R., Jafari Kashi, A.H., Lotfi, Z., Talebzadeh, S.M., Wickramatillake, A., Momtazan, M., Farsani, M.H., Marjani, S., Mobarak, S., 2020. The impact of sofosbuvir/daclatasvir or ribavirin in patients with severe COVID-19. J. Antimicrob. Chemother. 75, 3366–3372. https://doi.org/10.1093/jac/dkaa331.

Fong, P.C., Boss, D.S., Yap, T.A., Tutt, A., Wu, P., Mergui-Roelvink, M., Mortimer, P., Swaisland, H., Lau, A., O'Connor, M.J., Ashworth, A., Carmichael, J., Kaye, S.B., Schellens, J.H.M., de Bono, J.S., 2009. Inhibition of poly(ADP-Ribose) polymerase in tumors from BRCA mutation carriers. N. Engl. J. Med. 361, 123–134. https://doi.org/10.1056/nejmoa0900212.

Gao, Y., Yan, L., Huang, Y., Liu, F., Zhao, Y., Cao, L., Wang, T., Sun, Q., Ming, Z., Zhang, L., Ge, J., Zheng, L., Zhang, Y., Wang, H., Zhu, Y., Zhu, C., Hu, T., Hua, T., Zhang, B., Yang, X., Li, J., Yang, H., Liu, Z., Xu, W., Guddat, L.W., Wang, Q., Lou, Z., Rao, Z., 2020. Structure of the RNA-dependent RNA polymerase from COVID-19 virus. Science 368, 779–782. https://doi.org/10.1126/science.abb7498.

Gordon, D.E., Jang, G.M., Bouhaddou, M., Xu, J., Obernier, K., White, K.M., O'Meara, M. J., Rezelj, V.V., Guo, J.Z., Swaney, D.L., Tummino, T.A., Hüttenhain, R., Kaake, R. M., Richards, A.L., Tutuncuoglu, B., Foussard, H., Batra, J., Haas, K., Modak, M., Kim, M., Haas, P., Polacco, B.J., Braberg, H., Fabius, J.M., Eckhardt, M., Soucheray, M., Bennett, M.J., Cakir, M., McGregor, M.J., Li, Q., Meyer, B., Roesch, F., Vallet, T., Mac Kain, A., Miorin, L., Moreno, E., Naing, Z.Z.C., Zhou, Y., Peng, S., Shi, Y., Zhang, Z., Shen, W., Kirby, I.T., Melnyk, J.E., Chorba, J.S., Lou, K., Dai, S.A., Barrio-Hernandez, I., Memon, D., Hernandez-Armenta, C., Lyu, J., Mathy, C.J.P., Perica, T., Pilla, K.B., Ganesan, S.J., Saltzberg, D.J., Rakesh, R., Liu, X., Rosenthal, S.B., Calviello, L., Venkataramanan, S., Liboy-Lugo, J., Lin, Y., Huang, X.P., Liu, Y.F., Wankowicz, S.A., Bohn, M., Safari, M., Ugur, F.S., Koh, C., Savar, N.S., Tran, Q.D., Shengjuler, D., Fletcher, S.J., O'Neal, M.C., Cai, Y., Chang, J.

C.J., Broadhurst, D.J., Klippsten, S., Sharp, P.P., Wenzell, N.A., Kuzuoglu-Ozturk, D., Wang, H.Y., Trenker, R., Young, J.M., Cavero, D.A., Hiatt, J., Roth, T.L., Rathore, U., Subramanian, A., Noack, J., Hubert, M., Stroud, R.M., Frankel, A.D., Rosenberg, O. S., Verba, K.A., Agard, D.A., Ott, M., Emerman, M., Jura, N., von Zastrow, M., Verdin, E., Ashworth, A., Schwartz, O., d'Enfert, C., Mukherjee, S., Jacobson, M., Malik, H.S., Fujimori, D.G., Ideker, T., Craik, C.S., Floor, S.N., Fraser, J.S., Gross, J. D., Sali, A., Roth, B.L., Ruggero, D., Taunton, J., Kortemme, T., Beltrao, P., Vignuzzi, M., García-Sastre, A., Shokat, K.M., Shoichet, B.K., Krogan, N.J., 2020. A SARS-CoV-2 protein interaction map reveals targets for drug repurposing. Nat 459–468. https://doi.org/10.1038/s41586-020-2286-9, 2020 5837816 583.

Gribble, J., Stevens, L.J., Agostini, M.L., Anderson-Daniels, J., Chappell, J.D., Lu, X., Pruijssers, A.J., Routh, A.L., Denison, M.R., 2021. The coronavirus proofreading exoribonuclease mediates extensive viral recombination. PLoS Pathog. 17, e1009226 https://doi.org/10.1371/journal.ppat.1009226.

Huang, M., Zhang, W., Chen, H., Zeng, J., 2020. Targeting polyamine metabolism for control of human viral diseases. Infect. Drug Resist. 13, 4335. https://doi.org/10.2147/IDR.S262024.

Hui, D.S., I Azhar, E., Madani, T.A., Ntoumi, F., Kock, R., Dar, O., Ippolito, G., Mchugh, T. D., Memish, Z.A., Drosten, C., Zumla, A., Petersen, E., 2020. The continuing 2019-nCoV epidemic threat of novel coronaviruses to global health — the latest 2019 novel coronavirus outbreak in Wuhan, China. Int. J. Infect. Dis. https://doi.org/10.1016/j.ijid.2020.01.009.

Johnston, G.A.R., 2013. Advantages of an antagonist: bicuculline and other GABA antagonists. Br. J. Pharmacol. https://doi.org/10.1111/bph.12127.

Ju, J., Li, X., Kumar, S., Jockusch, S., Chien, M., Tao, C., Morozova, I., Kalachikov, S., Kirchdoerfer, R.N., Russo, J.J., 2020a. Nucleotide analogues as inhibitors of SARS-CoV Polymerase. Pharmacol. Res. Perspect. 8 https://doi.org/10.1002/prp2.674, 2020.03.12.989186.

Ju, J., Li, X., Kumar, S., Jockusch, S., Chien, M., Tao, C., Morozova, I., Kalachikov, S., Kirchdoerfer, R.N., Russo, J.J., 2020b. Nucleotide analogues as inhibitors of SARS-CoV Polymerase. Pharmacol. Res. Perspect. 8 https://doi.org/10.1002/prp2.674, 2020.03.18.997585.

Kang, J.I., Hong, J.Y., Choi, J.S., Lee, S.K., 2016. Columbianadin inhibits cell proliferation by inducing apoptosis and necroptosis in HCT116 colon cancer cells. Biomol. Ther. 24, 320–327. https://doi.org/10.4062/biomolther.2015.145.

Kim, Y., Jedrzejczak, R., Maltseva, N.I., Wilamowski, M., Endres, M., Godzik, A., Michalska, K., Joachimiak, A., 2020. Crystal structure of Nsp15 endoribonuclease NendoU from SARS-CoV-2. Protein Sci. 29, 1596–1605. https://doi.org/10.1002/pro.3873.

Kimberlin, D.W., Whitley, R.J., 2007. Antiviral therapy of HSV-1 and-2. In: Human Herpesviruses: Biology, Therapy, and Immunoprophylaxis. Cambridge University Press, pp. 1153–1174. https://doi.org/10.1017/CBO9780511545313.065.

Krainer, G., Broecker, J., Vargas, C., Fanghänel, J., Keller, S., 2012. Quantifying high-affinity binding of hydrophobic ligands by isothermal titration calorimetry. Anal. Chem. 84, 10715–10722. https://doi.org/10.1021/ac3025575.

Ksiazek, T.G., Erdman, D., Goldsmith, C.S., Zaki, S.R., Peret, T., Emery, S., Tong, S., Urbani, C., Comer, J.A., Lim, W., Rollin, P.E., Dowell, S.F., Ling, A.-E., Humphrey, C. D., Shieh, W.-J., Guarner, J., Paddock, C.D., Rota, P., Fields, B., DeRisi, J., Yang, J.-Y., Cox, N., Hughes, J.M., LeDuc, J.W., Bellini, W.J., Anderson, L.J., 2003. A novel coronavirus associated with severe acute respiratory syndrome. N. Engl. J. Med. 348, 1953–1966. https://doi.org/10.1056/nejmoa030781.

Kuiken, T., Fouchier, R.A.M., Schutten, M., Rimmelzwaan, G.F., Van Amerongen, G., Van Riel, D., Laman, J.D., De Jong, T., Van Doornum, G., Lim, W., Ling, A.E., Chan, P.K. S., Tam, J.S., Zambon, M.C., Gopal, R., Drosten, C., Van Der Werf, S., Escriou, N., Manuguerra, J.C., Stöhr, K., Peiris, J.S.M., Osterhaus, A.D.M.E., 2003. Newly discovered coronavirus as the primary cause of severe acute respiratory syndrome. Lancet 362, 263–270. https://doi.org/10.1016/S0140-6736(03)13967-0.

Lipinski, C.A., Lombardo, F., Dominy, B.W., Feeney, P.J., 1997. Experimental and computational approaches to estimate solubility and permeability in drug discovery and development settings. Adv. Drug Deliv. Rev. https://doi.org/10.1016/S0169-409X(96)00423-1.

Liu, C.J., Chen, P.J., Lai, M.Y., Kao, J.H., Jeng, Y.M., Chen, D.S., 2003. Ribavirin and interferon is effective for hepatitis C virus clearance in hepatitis B and C dually infected patients. Hepatology 37, 568–576. https://doi.org/10.1053/jhep.2003.50096.

Ma, Y., Wu, L., Shaw, N., Gao, Y., Wang, J., Sun, Y., Lou, Z., Yan, L., Zhang, R., Rao, Z., 2015. Structural basis and functional analysis of the SARS coronavirus nsp14-nsp10 complex. Proc. Natl. Acad. Sci. U. S. A. 112, 9436–9441. https://doi.org/10.1073/pnas.1508686112.

Malin, J.J., Suárez, I., Priesner, V., Fätkenheuer, G., Rybniker, J., 2021. Remdesivir against COVID-19 and other viral diseases. Clin. Microbiol. Rev. 34, 1–21. https://doi.org/10.1128/CMR.00162-20.

Masho, S.W., Wang, C.L., Nixon, D.E., 2007. Review of tenofovir-emtricitabine. Therapeut. Clin. Risk Manag.

Mercatelli, D., Giorgi, F.M., 2020. Geographic and genomic distribution of SARS-CoV-2 mutations. Front. Microbiol. 11, 1800. https://doi.org/10.3389/fmicb.2020.01800.

Mestdagh, N., Wülfert, E., 1999. Bicuculline increases Ca2+ transients in rat cerebellar granule cells through non-GABA(A) receptor associated mechanisms. Neurosci. Lett. 265, 95–98. https://doi.org/10.1016/S0304-3940(99)00213-X.

Mirza, M.U., Froeyen, M., 2020. Structural elucidation of SARS-CoV-2 vital proteins: computational methods reveal potential drug candidates against main protease, Nsp12 polymerase and Nsp13 helicase. J. Pharm. Anal. 10, 320–328. https://doi.org/10.1016/j.jpha.2020.04.008.

Moore, K., Colombo, N., Scambia, G., Kim, B.-G., Oaknin, A., Friedlander, M., Lisyanskaya, A., Floquet, A., Leary, A., Sonke, G.S., Gourley, C., Banerjee, S., Oza, A., González-Martín, A., Aghajanian, C., Bradley, W., Mathews, C., Liu, J., Lowe, E.S., Bloomfield, R., DiSilvestro, P., 2018. Maintenance olaparib in patients with newly diagnosed advanced ovarian cancer. N. Engl. J. Med. 379, 2495–2505. https://doi.org/10.1056/nejmoa1810858.

Morris, G.M., Huey, R., Lindstrom, W., Sanner, M.F., Belew, R.K., Goodsell, D.S., Olson, A.J., 2009. AutoDock4 and AutoDockTools4: automated docking with selective receptor flexibility. J. Comput. Chem. 30, 2785. https://doi.org/10.1002/JCC.21256.

Mudgal, R., Mahajan, S., Tomar, S., 2020. Inhibition of Chikungunya virus by an adenosine analog targeting the SAM-dependent nsP1 methyltransferase. FEBS Lett. 594, 678–694. https://doi.org/10.1002/1873-3468.13642.

Navarese, E.P., Musci, R.L., Frediani, L., Gurbel, P.A., Kubica, J., 2020. Ion channel inhibition against covid-19: a novel target for clinical investigation. Cardiol. J. 27, 421–424. https://doi.org/10.5603/CJ.a2020.0090.

Ou, X., Liu, Y., Lei, X., Li, P., Mi, D., Ren, L., Guo, L., Guo, R., Chen, T., Hu, J., Xiang, Z., Mu, Z., Chen, X., Chen, J., Hu, K., Jin, Q., Wang, J., Qian, Z., 2020. Characterization of spike glycoprotein of SARS-CoV-2 on virus entry and its immune cross-reactivity with SARS-CoV. Nat. Commun. 11, 1–12. https://doi.org/10.1038/s41467-020-15562-9.

O'Boyle, N.M., Banck, M., James, C.A., Morley, C., Vandermeersch, T., Hutchison, G.R., 2011. Open Babel: an open chemical toolbox. J. Cheminf. 3, 1–14. https://doi.org/10.1186/1758-2946-3-33.

Pareek, A., Kumar, R., Mudgal, R., Neetu, N., Sharma, M., Kumar, P., Tomar, S., 2022. Alphavirus antivirals targeting RNA-dependent RNA polymerase domain of nsP4 divulged using surface plasmon resonance. FEBS J. 289, 4901–4924. https://doi.org/10.1111/febs.16397.

Parker, M.M., Masters, P.S., 1990. Sequence comparison of the N genes of five strains of the coronavirus mouse hepatitis virus suggests a three domain structure for the nucleocapsid protein. Virology 179, 463–468. https://doi.org/10.1016/0042-6822(90)90316-J.

Pelaez, A., Lyon, G.M., Force, S.D., Ramirez, A.M., Neujahr, D.C., Foster, M., Naik, P.M., Gal, A.A., Mitchell, P.O., Lawrence, E.C., 2009. Efficacy of oral ribavirin in lung transplant patients with respiratory syncytial virus lower respiratory tract infection. J. Heart Lung Transplant. 28, 67–71. https://doi.org/10.1016/j.healun.2008.10.008.

Ratjen, F., Hug, C., Marigowda, G., Tian, S., Huang, X., Stanojevic, S., Milla, C.E., Robinson, P.D., Waltz, D., Davies, J.C., Rosenfeld, M., Starner, T., Retsch-Bogart, G., Chmiel, J., Orenstein, D., Milla, C., Rubenstein, R., Walker, S., Cornell, A., Asfour, F., Black, P., Colombo, J., Froh, D., McColley, S., Ruiz, F., Quintero, D., Casey, A., Mueller, G., Flume, P., Livingston, F., Rock, M., O'Sullivan, B., Schmidt, H., Lahiri, T., McNamara, J., Chidekel, A., Sass, L., Keens, T., Schaeffer, D., Solomon, M., Chilvers, M., Lands, L., Junge, S., Griese, M., Staab, D., Pressler, T., van Koningsburggen-Rietschel, S., Naehrlich, L., Reid, A., Balfour-Lynn, I., Urquhart, D., Lee, T., Munck, A., Gaudelus, I.S., De Boeck, C., Reix, P., Malfroot, A., Bui, S., Selvadurai, H., Robinson, P., Wainwright, C., Clements, B., Hilton, J., Hjelte, L., 2017. Efficacy and safety of lumacaftor and ivacaftor in patients aged 6–11 years with cystic fibrosis homozygous for F508del-CFTR: a randomised, placebo-controlled phase 3 trial. Lancet Respir. Med. 5, 557–567. https://doi.org/10.1016/S2213-2600(17)30215-1.

Robson, M., Im, S.-A., Senkus, E., Xu, B., Domchek, S.M., Masuda, N., Delaloge, S., Li, W., Tung, N., Armstrong, A., Wu, W., Goessl, C., Runswick, S., Conte, P., 2017. Olaparib for metastatic breast cancer in patients with a germline BRCA mutation. N. Engl. J. Med. 377, 523–533. https://doi.org/10.1056/nejmoa1706450.

Rosas-Lemus, M., Minasov, G., Shuvalova, L., Inniss, N.L., Kiryukhina, O., Brunzelle, J., Satchell, K.J.F., 2020. High-resolution structures of the SARS-CoV-2 2′-O-methyltransferase reveal strategies for structure-based inhibitor design. Sci. Signal. 13, 1202. https://doi.org/10.1126/scisignal.abe1202.

Safari, I., Elahi, E., 2022. Evolution of the SARS-CoV-2 genome and emergence of variants of concern. Arch. Virol. https://doi.org/10.1007/s00705-021-05295-5.

Sette, A., Crotty, S., 2021. Adaptive Immunity to SARS-CoV-2 and COVID-19. Cell. https://doi.org/10.1016/j.cell.2021.01.007.

Shapiro, D., Stevens, D., Stahl, S.M., 2017. Flibanserin–the female viagra? Int. J. Psychiatr. Clin. Pract. https://doi.org/10.1080/13651501.2017.1315138.

Sharma, R., Fatma, B., Saha, A., Bajpai, S., Sistla, S., Dash, P.K., Parida, M., Kumar, P., Tomar, S., 2016. Inhibition of chikungunya virus by picolinate that targets viral capsid protein. Virology 498, 265–276. https://doi.org/10.1016/j.virol.2016.08.029.

Sharma, R., Kesari, P., Kumar, P., Tomar, S., 2018. Structure-function insights into chikungunya virus capsid protein: small molecules targeting capsid hydrophobic pocket. Virology 515, 223–234. https://doi.org/10.1016/J.VIROL.2017.12.020.

Simonis, A., Theobald, S.J., Fätkenheuer, G., Rybniker, J., Malin, J.J., 2021. A comparative analysis of remdesivir and other repurposed antivirals against SARS-CoV-2. EMBO Mol. Med. 13, e13105 https://doi.org/10.15252/emmm.202013105.

Singh, H., Mudgal, R., Narwal, M., Kaur, R., Singh, V.A., Malik, A., Chaudhary, M., Tomar, S., 2018. Chikungunya virus inhibition by peptidomimetic inhibitors targeting virus-specific cysteine protease. Biochimie 149, 51–61. https://doi.org/10.1016/j.biochi.2018.04.004.

Singhal, T., 2020. A review of coronavirus disease-2019 (COVID-19). Indian J. Pediatr. https://doi.org/10.1007/s12098-020-03263-6.

Smee, D.F., Wong, M.H., Bailey, K.W., Sidwell, R.W., 2006. Activities of oseltamivir and ribavirin used alone and in combination against infections in mice with recent isolates of influenza A (H1N1) and B viruses. Antivir. Chem. Chemother. 17, 185–192. https://doi.org/10.1177/095632020601700403.

Su, X., Wu, B., Zhang, W., Ji, Y.H., Wang, Q., Tan, Z.Y., 2019. Inhibitory effects of columbianadin on nociceptive behaviors in a neuropathic pain model, and on voltage-gated calcium currents in dorsal root ganglion neurons in mice. Front. Pharmacol. 10, 1522. https://doi.org/10.3389/fphar.2019.01522.

Svensson, L., Camejo, G., Cabré, A., Vallvé, J.C., Pedreño, J., Norén, K., Wiklund, O., Hultén, L.M., 2003. Fatty acids modulate the effect of darglitazone on macrophage CD36 expression. Eur. J. Clin. Invest. 33, 464–471. https://doi.org/10.1046/j.1365-2362.2003.01181.x.

Temesgen, Z., Talwani, R., Rizza, S.A., 2014. Sofosbuvir for the treatment of chronic hepatitis C virus infection. Drugs Today 50, 421–434. https://doi.org/10.1358/dot.2014.50.6.2141371.

Trott, O., Olson, A.J., 2010. AutoDock Vina: improving the speed and accuracy of docking with a new scoring function, efficient optimization and multithreading. J. Comput. Chem. 31, 455. https://doi.org/10.1002/JCC.21334.

Vallejos, X., Wu, C., 2017. Flibanserin: a novel, nonhormonal agent for the treatment of hypoactive sexual desire disorder in premenopausal women. J. Pharm. Pract. https://doi.org/10.1177/0897190016630409.

Vansteenkiste, J.F., Van De Kerkhove, C., Wauters, E., Van Mol, P., 2019. Capmatinib for the treatment of non-small cell lung cancer. Expert Rev. Anticancer Ther. 19, 659–671. https://doi.org/10.1080/14737140.2019.1643239.

Varma, A.K., Patil, R., Das, S., Stanley, A., Yadav, L., Sudhakar, A., 2010. Optimized hydrophobic interactions and hydrogen bonding at the target-ligand interface leads the pathways of Drug-Designing. PLoS One 5, e12029. https://doi.org/10.1371/journal.pone.0012029.

Wallace, A.C., Laskowski, R.A., Thornton, J.M., 1995. Ligplot: a program to generate schematic diagrams of protein-ligand interactions. Protein Eng. Des. Sel. 8, 127–134. https://doi.org/10.1093/protein/8.2.127.

Wang, C., Horby, P.W., Hayden, F.G., Gao, G.F., 2020. A novel coronavirus outbreak of global health concern. Lancet. https://doi.org/10.1016/S0140-6736(20)30185-9.

Wilhelmus, K.R., 2015. Antiviral treatment and other therapeutic interventions for herpes simplex virus epithelial keratitis. Cochrane Database Syst. Rev. https://doi.org/10.1002/14651858.CD002898.pub5.

Wilkinson, A.J., Fersht, A.R., Blow, D.M., Carter, P., Winter, G., 1984. A large increase in enzyme-substrate affinity by protein engineering. Nature 307, 187–188. https://doi.org/10.1038/307187a0.

Wu, A., Peng, Y., Huang, B., Ding, X., Wang, X., Niu, P., Meng, J., Zhu, Z., Zhang, Z., Wang, J., Sheng, J., Quan, L., Xia, Z., Tan, W., Cheng, G., Jiang, T., 2020. Genome composition and divergence of the novel coronavirus (2019-nCoV) originating in China. Cell Host Microbe 27, 325–328. https://doi.org/10.1016/J.CHOM.2020.02.001.

Zaki, A.M., van Boheemen, S., Bestebroer, T.M., Osterhaus, A.D.M.E., Fouchier, R.A.M., 2012. Isolation of a novel coronavirus from a man with pneumonia in Saudi Arabia. N. Engl. J. Med. 367, 1814–1820. https://doi.org/10.1056/nejmoa1211721.

Zhang, L., Lou, W.H., Xu, X.F., Wu, W., Rong, Y.F., Jin, D.Y., 2017. SN38 increases IL-8 expression through the MAPK pathways in HCT8 cells. Int. J. Mol. Med. 39, 217–222. https://doi.org/10.3892/ijmm.2016.2810.

Zhang, L., Lin, D., Sun, X., Rox, K., Hilgenfeld, R., 2020. X-ray structure of main protease of the novel coronavirus SARS-CoV-2 enables design of α-ketoamide inhibitors. bioRxiv 1–14. https://doi.org/10.1101/2020.02.17.952879.

Zheng, S., Xu, S., Wang, G., Tang, Q., Jiang, X., Li, Z., Xu, Y., Wang, R., Lin, F., 2017. Proposed hydrogen-bonding index of donor or acceptor reflecting its intrinsic contribution to hydrogen-bonding strength. J. Chem. Inf. Model. 57, 1535–1547. https://doi.org/10.1021/acs.jcim.7b00022.

Zhou, P., Yang, X. Lou, Wang, X.G., Hu, B., Zhang, L., Zhang, W., Si, H.R., Zhu, Y., Li, B., Huang, C.L., Chen, H.D., Chen, J., Luo, Y., Guo, H., Jiang, R. Di, Liu, M.Q., Chen, Y., Shen, X.R., Wang, X., Zheng, X.S., Zhao, K., Chen, Q.J., Deng, F., Liu, L.L., Yan, B., Zhan, F.X., Wang, Y.Y., Xiao, G.F., Shi, Z.L., 2020. A pneumonia outbreak associated with a new coronavirus of probable bat origin. Nature 579, 270–273. https://doi.org/10.1038/s41586-020-2012-7.